earth

MDPI

Article

Physical–Statistical Characterization of PM_{10} and $PM_{2.5}$ Concentrations and Atmospheric Transport Events in the Azores During 2024

Maria Gabriela Meirelles [1,2] and Helena Cristina Vasconcelos [1,3,*]

[1] Faculty of Science and Technology, University of the Azores, 9500-321 Ponta Delgada, Portugal; maria.gf.meirelles@uac.pt
[2] Research Institute of Marine Sciences, University of the Azores (OKEANOS), 9901-862 Horta, Portugal
[3] Laboratory of Instrumentation, Biomedical Engineering and Radiation Physics (LIBPhys, UNL), Department of Physics, NOVA School of Science and Technology, 2829-516 Caparica, Portugal
* Correspondence: helena.cs.vasconcelos@uac.pt

Abstract: This study presented a comprehensive physical–statistical analysis of atmospheric particulate matter (PM_{10} and $PM_{2.5}$) and trace gases (SO_2 and O_3) over Faial Island in the Azores archipelago during 2024. We collected real-time data at the Espalhafatos rural background station, covering 35,137 observations per pollutant, with 15 min intervals. Descriptive statistics, probability distribution fitting (Normal, Lognormal, Weibull, Gamma), and correlation analyses were employed to characterize pollutant dynamics and identify extreme pollution episodes. The results revealed that $PM_{2.5}$ (fine particles) concentrations are best modeled by a Lognormal distribution, while PM_{10} concentrations fit a Gamma distribution, highlighting the presence of heavy-tailed, positively skewed behavior in both cases. Seasonal and episodic variability was significant, with multiple Saharan dust transport events contributing to PM exceedances, particularly during winter and spring months. These events, confirmed by CAMS and SKIRON dust dispersion models, affected not only southern Europe but also the Northeast Atlantic, including the Azores region. Weak to moderate correlations were observed between PM concentrations and meteorological variables, indicating complex interactions influenced by atmospheric stability and long-range transport processes. Linear regression analyses between SO_2 and O_3, and between SO_2 and $PM_{2.5}$, showed statistically significant but low-explanatory relationships, suggesting that other meteorological and chemical factors play a dominant role. This result highlights the importance of developing air quality policies that address both local emissions and long-range transport phenomena. They support the implementation of early warning systems and health risk assessments based on probabilistic modeling of particulate matter concentrations, even in remote Atlantic locations such as the Azores.

Keywords: particulate matter ($PM_{2.5}$, PM_{10}); air quality; Saharan dust transport; statistical models; Azores; atmospheric pollutants (O_3, SO_2); insular environments; environmental risk

check for updates

Academic Editors: Charles Jones and Carmine Serio

Received: 1 May 2025
Revised: 26 May 2025
Accepted: 5 June 2025
Published: 6 June 2025

Citation: Meirelles, M.G.; Vasconcelos, H.C. Physical–Statistical Characterization of PM_{10} and $PM_{2.5}$ Concentrations and Atmospheric Transport Events in the Azores During 2024. *Earth* **2025**, *6*, 54. https://doi.org/10.3390/earth6020054

Copyright: © 2025 by the authors. Licensee MDPI, Basel, Switzerland. This article is an open access article distributed under the terms and conditions of the Creative Commons Attribution (CC BY) license (https://creativecommons.org/licenses/by/4.0/).

1. Introduction

Air quality deteriorates with the increase in emissions of atmospheric pollutants, contributing negatively to human health and the balance of ecosystems. Kumar et al. [1] examined that the alarming degradation of air quality, atmospheric conditions, economy, and human life due to air pollution needs significant in-depth studies to ascertain causes, contributions, and impacts for developing and implementing an effective policy to combat these

issues. Air pollution is responsible worldwide for 9–12 million deaths annually. Hening [2] investigated that the major contributor to air pollution is particulate matter ≤2.5 μg per cubic meter of air ($PM_{2.5}$) from vehicles, industrial emissions, and wildfire smoke. Nguyen et al. [3] verified that an extensive body of literature has concluded that exposure to air pollution is associated with an increased risk of respiratory hospital admissions in children worldwide. Vallero [4] proposed that exposure to elevated concentrations of tropospheric (ground-level) ozone is particularly harmful to people with asthma or lung disease and children who are more likely than adults to have asthma, which is aggravated by ozone. Prolonged exposure to air pollutants, such as particulate matter (PM), is associated with respiratory and cardiovascular diseases and significant environmental impacts. Among the main types of particles suspended in the air, PM_{10} (particles with an aerodynamic diameter $\leq$ 10 μm) and $PM_{2.5}$ (fine particles with an aerodynamic diameter $\leq$ 2.5 μm) stand out, which have different behaviors in the atmosphere, due to their diameter, their concentration, and their chemical behavior. Wei et al. [5] verified that atmospheric pressure and rainfall were negatively correlated with $PM_{2.5}$, with notable reductions in concentrations under high-pressure conditions and rainfall levels between 0 and 20 mm. Son et al. [6] concluded that annual assessments indicated that $PM_{2.5}$ concentrations in Thailand reached 21.4 $\mu g/m^3$ in 2020, making it the 34th most polluted country in the world. Alves et al. [7] investigated the toxicity, and consequently the health effects, of $PM_{2.5}$ is highly dependent on its chemical composition. According to Dawidowski et al. [8], in addition to health effects, $PM_{2.5}$ can generate varied climatic and hydrological effects, as it has the potential to alter the amount of solar radiation incident on the surface, alter the distribution of solar energy in the atmosphere, and alter the growth and hygroscopic activity of the cloud condensation nucleus. Wei et al. [9] onducted a series of experimental studies and verified that $PM_{2.5}$ is influenced by complex factors, including meteorological conditions, socio-economic activities, and industrial emissions, making accurate predictions essential for managing air quality and mitigating health risks. Chen et al. [10] investigated and proposed that $PM_{2.5}$ is a complex mixture composed of chemical components from various sources, each with unique physical properties and uncertain toxicity. Particulate matter is composed of a complex heterogeneous mixture originating from combustion processes, pollen, sea salt, volcanic ash, suspended dust, industrial activities, and vehicle transport processes, with variable composition and concentration in time and space. Its origin is attributed to natural and anthropogenic sources.

In island regions, such as the Azores, air quality is influenced by meteorological factors, local emissions, and long-distance atmospheric transport processes. The presence of suspended particles can be affected by the action of winds, relative humidity, and the occurrence of natural phenomena, such as dust storms coming from the Sahara, or even resulting from fires on the American continent. Furthermore, the formation and dispersion of these particles are directly related to physical and chemical processes that occur in the atmosphere, including photochemical reactions. Li et al. [11] concluded that $PM_{2.5}$ shows different growth rates at different accumulation stages and may undergo slow to explosive growth depending on the presence of the precursor. Zhen et al. [12] examined that atmospheric particulate matter comprises organic materials, water-soluble inorganic ions, and other substances, making it a comprehensive mixture. It is also composed of metallic elements, which are highly dangerous even in low concentrations.

In this study, we also paid attention to PM_{10}. Canu et al. and Shams et al. [13,14] intensely investigated that exposure to ambient PM_{10} may increase the risk of chronic obstructive pulmonary disease (COPD) and lung function decline. According to Alves et al. [15], in fact, it is well known that particulate matter with a diameter lower than 10 or 2.5 μm (PM_{10} and $PM_{2.5}$, respectively) poses serious health risks. Due to their small size,

these particles can penetrate deep into the lungs, leading to a variety of respiratory and cardiovascular diseases. According to Núnez [16], the profile of PM_{10} in the ambient air of Faial Island is determined by various sources and factors that depend on the region's characteristics. During 2024, there were four times that these particles showed an abnormal value, greater than the mean. These episodes are related to the transport of natural particles with origin from arid regions. In this context, dust storms are particularly interesting because they spread large quantities of mineral particles from arid areas of the planet, which are deposited in distant areas. According to Neff et al. [17], these relatively small particles receive much attention because they can travel thousands of kilometers through the atmosphere, and they play a major role in the radiative forcing of the atmosphere, thereby affecting climate.

The statistical characterization of PM_{10} and $PM_{2.5}$ concentrations is essential to understand their temporal variability and identify patterns of occurrence of extreme events. The application of models such as the Lognormal distribution and the Weibull distribution is widely used to describe the behavior of these particles in the atmosphere. Wang et al. [18] investigated that the PM_{10} concentration distribution was simulated using the Lognormal, Weibull, and Gamma distributions, and the best statistical distribution of PM_{10} concentration in the 5 cities was detected using the sharpest method. The average daily concentration of PM_{10} in the five cities was fitted using the Lognormal distribution. According to Lu [19], based on the statistical properties (probability density) of air pollutants, it is easy to estimate how many times the exceedance compared with air quality standards occurs. In this paper, three distributions (Lognormal, Weibull, and V-type distribution) were used to simulate the PM_{10} concentration distribution in areas of Taiwan. The Lognormal distribution is the most popular distribution used to adjust the concentration of air pollutants. Mijić et al. [20] proposed that Lognormal, Weibull, and type V distributions were chosen to fit the data for PM_{10} in Belgrade. On the other hand, Sánchez [21], the literature shows that the distribution of $PM_{2.5}$ concentration recorded by eight air quality monitoring stations during 2021, covering a large part of the metropolitan region of Santiago de Chile, can be explained by a q-Weibull function. The q-Weibull function is a generalization of the Weibull distribution.

Kunecki et al. [22] proposed that these types of matter ($PM_{2.5}$ and PM_{10}) are also subjected to different processes of formation and removal from the atmosphere and have a different impact on human health due to varying degrees of absorption and accumulation in the respiratory system. Depending on their origin, they can form separate populations: nucleation mode particles, Aitken mode particles, and accumulation mode particles. Yang et al. [23] said that in this sense, analyzing the correlation between pollutants and meteorological variables also makes it possible to evaluate the main factors that influence their concentrations over time. Interactions between $PM_{2.5}$ and meteorological factors play a crucial role in air pollution analysis. Pateraki et al. [24] investigated that fine particles having longer residence time in the atmosphere and being mainly influenced by long-range transport proved to be less susceptible than the bigger ones not only to the meteorological parameters' fluctuations but also to the different circulation types. Li et al. [25] examined that annual PM concentrations were negatively correlated with annual precipitation, wind speed, and relative humidity, but were positively correlated with annual atmospheric pressure. Chen et al. [26] this study showed that high temperature, humidity, and low rainfall increased the risk of obstructive lung disease. Synergistic effects were observed between temperature, SO_2, and $PM_{2.5}$. The impact of air pollutants on obstructive lung disease must consider these interactions. Lei et al. [27] proposed that temperature was a significant meteorological parameter influencing the correlation between $PM_{2.5}$ and O_3 concentrations, with a coefficient of determination (R^2) of 0.83. Under high-temperature

conditions, $PM_{2.5}$ and O_3 concentrations exhibited a stronger positive correlation. Carvalho et al. [28] investigated that with respect to serious pathologies (asthma, pneumonia, and rhinitis) the results indicate that the presence of primary pollutants such as NO_2 and SO_2 in the winter and spring months, may contribute to a greater number of individuals with pathologies in the study. Interestingly, PM_{10} is not dependent on these pathologies. Meirelles et al. [29] show that the study mentioned here provides comparison evidence of the significant influence of meteorological variables and air quality on hospital admissions for cardiovascular diseases, hypertension, and circulatory system in Faial Island, Azores, over the period 2010 to 2019. Carvalho et al. [30] proposed that results suggest associations between pneumonia and asthma with high SO2 concentrations, positive correlation of surface O_3 concentrations with rhinitis cases, and negative correlation with NO_2. PM_{10} has a small negative correlation with pneumonia. All three diseases correlate with each other as well as with O_3 and SO_2.

This study aims to analyze the time series of PM_{10} and $PM_{2.5}$ on Faial Island, in the Azores archipelago, throughout the year 2024. The research investigates the occurrence of episodes of particulate matter exceedances, identifies statistical patterns, and evaluates the relationship between concentrations of particulate matter, meteorological factors (temperature, pressure, wind speed, and relative humidity), and atmospheric trace gases (O_3 and SO_2). Additionally, statistical distributions are applied to model the data and interpret the physical processes underlying the dispersion and removal of these particles from the atmosphere.

Despite the well-documented health and environmental effects of PM_{10} and $PM_{2.5}$ in urban and industrialized areas, studies on air quality in islands remain scarce. The Azores, located between Europe and the United States, provide a unique setting to investigate the interplay between local emissions, long-range transport of natural aerosols (e.g., Saharan dust, wildfire plumes), and meteorological variability. This study aims to fill this gap by analyzing the temporal variability of PM concentrations in Faial Island and applying statistical models to identify key atmospheric drivers of air pollution in an island context.

Therefore, the main objectives of this study are: (i) to identify and characterize critical pollution episodes involving PM_{10}, $PM_{2.5}$, SO_2, and O_3 concentrations during 2024; (ii) to apply and compare statistical distribution models suited to episodic and skewed environmental data; (iii) to examine exceedance events in relation to atmospheric transport phenomena, particularly Saharan dust intrusions; (iv) to assess how meteorological variables influenced pollutant peaks, despite limitations in year-round data coverage.

2. Data Collection, Methods, and Processing

2.1. Study Area and Dataset

The Azores are a Portuguese archipelago located in the North Atlantic Ocean Basin, approximately between 39°43′ and 36°55′ north latitude and 24°46′ to 31°16′ west longitude. The archipelago is made up of nine islands, divided into three groups: the eastern group: São Miguel and Santa Maria; the central group: Terceira, Graciosa, São Jorge, Pico, and Faial; and the western group: Flores and Corvo. This archipelago is located approximately 1500 km west of the city of Lisbon and approximately 3900 km off the east coast of North America, it is shown in Figure 1. The strategic position of the islands allows them to be an important point for climate and oceanic studies, presenting a unique environment due to their volcanic origin and isolated location in the Atlantic.

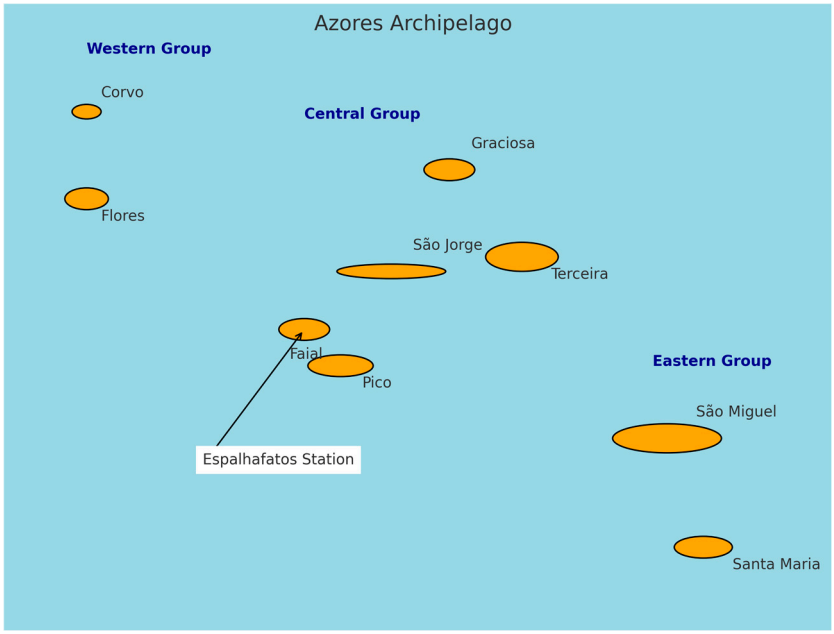

Figure 1. Location of the Azores archipelago.

The Azores Archipelago, with a total area of 2322 km^2, is significantly influenced by the Azores High (or Azores Anticyclone), a semi-permanent high-pressure system located in the North Atlantic. This system plays a crucial role in shaping the climate not only of the Azores but also of surrounding regions across the Atlantic basin. According to the NCEP/NCAR reanalysis data (1961–1990) from the National Centers for Environmental Prediction and the National Center for Atmospheric Research, the Azores High is typically centered near the archipelago or to its southwest (SW) or south (S) throughout most of the year. However, during the months of November to January, the center of this anticyclone tends to shift toward the south or southeast (SE). This system is more intense and developed in the summer months when its action extends to around 45°N, being less intense and developed in spring and autumn. The major axis of the Anticyclone is normally oriented in a Southwest-Northeast direction, except in the months of October to December when the orientation is approximately West to East.

According to Meirelles et al. [31], the prevailing atmospheric conditions in the Azores are primarily influenced by the position and intensity of the Azores High, the dynamics of the depressions along the Polar Front, and the moderating effect of the ocean—particularly due to the influence of the warm Gulf Stream. Carvalho et al. [32] further emphasize that the archipelago's proximity to the North Atlantic Subtropical Anticyclone (commonly known as the Azores High) has established the region as a key reference point for the characterization of atmospheric circulation patterns that influence weather in Western Europe.

Air quality analysis in the Azores region is carried out by monitoring primary pollutants (emitted directly into the atmosphere), secondary pollutants (resulting from photochemical reactions, for example) and particulate matter: nitrogen dioxide (NO_2), sulfur dioxide (SO_2), fine suspended particles with a diameter of less than 10 µm (PM_{10}) and a diameter of less than 2.5 µm ($PM_{2.5}$), tropospheric ozone (O_3) and carbon monoxide (CO). This analysis is based on the characterization carried out at the monitoring station located on the island of Faial, in Espalhafatos, which began sampling in April 2006 and is part of the country's monitoring network. The station has five automatic analyzers that allow continuous and real-time monitoring of pollutants. This rural background station is the only one representing the Azores Region in the National Ambient Air Quality Monitoring Network. In addition, it measures meteorological parameters such as wind

speed, temperature, relative humidity, precipitation, and solar radiation. The collected data are validated and sent to QualAr [33], the national air quality database, where daily air quality indices and other statistical parameters are made available. Air quality analysis reports are prepared annually. Continuous monitoring of air quality in the region aims to prevent harmful effects on human health and the environment, ensuring that updated information is made available to the public. In the assessment and management of air quality, at least the following pollutants must be considered: sulfur dioxide (SO_2), nitrogen dioxide (NO_2), nitrogen oxides (NO_x), suspended particles (PM_{10} and $PM_{2.5}$), lead (Pb), benzene (C_6H_6), carbon monoxide (CO), ozone (O_3), arsenic (As), cadmium (Cd), nickel (Ni) and mercury (Hg).

In this study, we used data for SO_2, O_3, $PM_{2.5}$, and PM_{10}, measured with certified analyzers: UV fluorescence (TUV-Report 936/21206773/CEN 14212) for SO_2, UV absorption (TUV-Report 936/21205818/CEN 14625) for O_3, and beta radiation (RC 21195EN 14907) for both $PM_{2.5}$ and PM_{10}. The time series of these pollutants was analyzed using 15 min intervals over the full year of 2024. Concentrations observed in ambient air reflect both local emissions and long-range transport processes—including contributions from Saharan dust events and biomass burning in South America, which frequently affect the Azores region.

To explore annual patterns and variability, Figure 2 displays scatter plots with linear trend lines for $PM_{2.5}$, PM_{10}, SO_2, and O_3 concentrations throughout 2024.

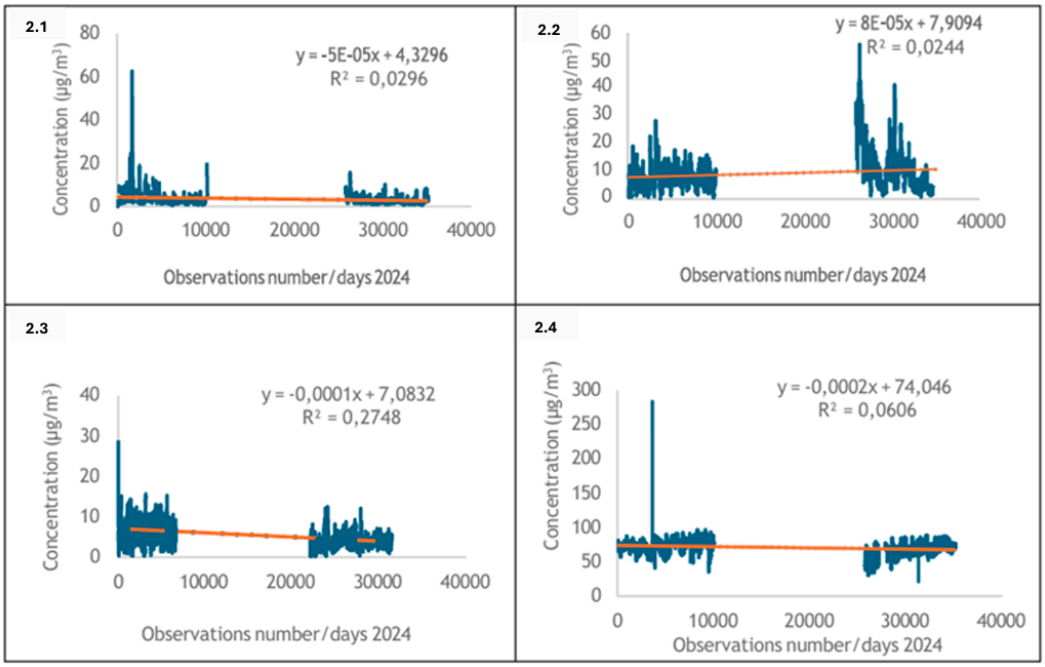

Figure 2. Concentrations observed at Espalhafatos station (2024): (**2.1**) $PM_{2.5}$, (**2.2**) PM_{10}, (**2.3**) SO_2, and (**2.4**) O_3.

The time series for each pollutant included a theoretical maximum of 35,137 15-min observations for the year. The time series for each pollutant included a theoretical maximum of 35,137 15 min observations for the year. However, actual data availability was highly uneven across the months. For $PM_{2.5}$, valid data were only available for January, February, April, August, and December, with no records from March, May, June, July, September, October, or November. For PM_{10}, data were available from January to May only, with no observations from June through December. Similarly, SO_2 and O_3 data were recorded only between January and May, with a complete absence during the second half of the year.

These extended data gaps—particularly between spring and autumn—prevent a robust assessment of seasonal variability. Accordingly, the study does not aim to characterize

full-year pollutant trends but rather focuses on critical pollution episodes occurring during periods with confirmed data availability. This limitation is explicitly acknowledged and considered throughout the analytical design, discussion, and conclusion.

To ensure analytical robustness and avoid introducing bias, a complete-case analysis strategy was adopted. No imputation techniques were applied. All descriptive statistics and probability distributions were calculated using the available data for each pollutant individually. For correlation and regression analyses involving multiple pollutants, only time-aligned entries with complete hourly data (n = 20,265) were used. This approach ensures that results reflect actual measurements and avoids the risks associated with imputing values in environmental time series, where missingness may be non-random and related to instrumental or meteorological disruptions.

2.2. Descriptive Statistics for Pollutant Concentration

For the statistical analysis of particulate matter (PM_{10} and $PM_{2.5}$) and primary (SO_2) and secondary (O_3) pollutants, the mean, median, standard deviation, mode, variance, kurtosis, and the 25th, 50th, and 75th percentiles were calculated.

2.3. Performance Indicator: Coefficient of Determination

The coefficient of determination R^2 was calculated to verify what proportion of the data variability is explained by the linear regression model. In the context of the time series, it evaluates how well the model can represent observed values over time.

2.4. Probability Distributions

Four theoretical distributions, namely Weibull, Gamma, Normal, and Lognormal distributions, are used to fit the entire measured $PM_{2.5}$ and PM_{10} data. Abdullah [34] used for parameter estimation; the method of maximum likelihood estimation was selected.

The selection of the Lognormal, Gamma, Weibull, and Normal distributions was based on their historical and theoretical suitability for modeling air pollutant concentrations, particularly those characterized by right-skewed behavior and high variability. The Lognormal distribution is widely used in air quality studies for $PM_{2.5}$ due to its ability to model non-negative, positively skewed data arising from multiple small-scale sources and occasional high-emission events. The Gamma distribution is often employed for PM_{10}, especially in regions affected by episodic dust intrusions, as it captures heavy-tailed behavior well. Weibull distribution is commonly applied in environmental statistics due to its flexibility in modeling skewed data, and the Normal distribution was included for comparative purposes, despite its limitations with skewed datasets. These choices are well supported in the literature by Zhang et al. [35] and Noor et al. [36] and were validated in this study through Kolmogorov–Smirnov tests, AIC, and BIC criteria.

2.5. Exceedances: $PM_{2.5}$, PM_{10}, SO_2, and O_3 Overview

After accessing the Air Quality Monitoring Portal in the Autonomous Region of the Azores (PMQA) [37] and reviewing the dates of $PM_{2.5}$ and PM_{10} exceedance alerts, moderate and severe outliers were identified in the 2024 time series of particulate matter, SO_2, and O_3. For some exceedance periods, Pearson's correlation coefficients were calculated between the parameters studied.

3. Results

3.1. Descriptive Statistics and Variability

3.1.1. Summary of Data and Missing Values

The analyzers installed at the Espalhafatos station measure air pollutants every 15 min. For one year, 35.137 values are recorded for each pollutant. However, in the series used in this study, there is a significant amount of missing data, ranging from 16.593 (PM_{10}) to 20.248 (SO_2). As the interest of this study is centered on some periods of the year, those in which alerts were issued due to excess particles in the atmosphere, we consider that the reliability of the analysis is assured. Table 1 shows the values obtained from the statistical analysis carried out on the time series under study.

Table 1. Descriptive statistics for $PM_{2.5}$, PM_{10}, SO_2, and O_3 concentrations ($\mu g/m^3$) recorded at the Espalhafatos station (Faial Island) during 2024. The statistics include mean, median, standard deviation, mode, variance, kurtosis, minimum, maximum, and percentiles (25th, 50th, 75th). All values are expressed in $\mu g/m^3$.

Station Espalhafatos Faial (2024)					
		$PM_{2.5}$	**PM_{10}**	**SO_2**	**O_3**
Total Data		35,137	35,137	35,137	35,137
Missing Data		17,859	16,593	20,248	16,637
Mean		3.42	9.29	5.34	70.97
Median		2.48	7.91	5.0	72.1
Standard Deviation		3.64	6.83	2.37	9.74
Mode		1.59	10.2	5.0	70.6
Variance		13.25	46.67	5.61	94.92
Kurtosis		85.31	6.08	2.12	14.17
Minimum Value		0.4	0.49	0.02	9.74
Maximum Value		62.7	56.2	28.9	284
Range					
Percentiles	25	1.59	4.77	3.57	66.2
	50	3.42	9.29	5.34	70.97
	75	4.13	11.5	6.69	77.5

During the year 2024, the concentration of half of the $PM_{2.5}$ performed showed concentrations below 2.48 $\mu g/m^3$. A kurtosis equal to 85.31 $\mu g/m^3$ indicates a distribution with very long tails, that is, there are rare events of concentrations with high values. Most $PM_{2.5}$ is at low levels, but there are sporadic events of high concentration, which justifies the high kurtosis.

A standard deviation equal to 6.83 $\mu g/m^3$ indicates that the values obtained for the PM_{10} time series have greater variability than the values analyzed in the $PM_{2.5}$ series. A kurtosis value of 6.08 $\mu g/m^3$ suggests that PM_{10} particulate matter has a slightly asymmetric distribution with some extreme measurements. The PM_{10} time series shows greater variation than the $PM_{2.5}$ time series, indicating more pronounced pollution episodes, but within generally low limits.

The values of SO_2 concentrations throughout the year 2024 showed average values equal to 5.34 $\mu g/m^3$, with relatively low variability (standard deviation equal to 2.37 $\mu g/m^3$), and 75% of the measurements are below 6.69 $\mu g/m^3$. The concentration

of SO_2 appears to be relatively uniformly distributed, without large peaks or extreme variations. Most values remain close to the average.

The time series of O_3 concentration values indicates that half of the data analyzed presented values below 72.1 $\mu g/m^3$. A standard deviation equal to 9.74 $\mu g/m^3$ indicates significant variability for these data. 14.17 $\mu g/m^3$ is the kurtosis value, indicating the presence of extremely high concentration events. O_3 has high average concentrations. Regions with low primary pollution may have higher average O_3 levels due to their secondary formation process and the lower presence of NO, which could remove it from the atmosphere. Kurtosis suggests the occurrence of high peaks that may pose health risks.

The air quality parameters analyzed at the Espalhafatos station suggest acceptable levels most of the time, but there are episodes of high concentration, especially for $PM_{2.5}$ and O_3. The significant volume of missing data may constrain the accuracy of statistical analyses and seasonal pattern interpretations. The high kurtosis value for $PM_{2.5}$ and O_3 suggests that there are specific periods of air quality deterioration, which may be related to meteorological events or intermittent emission sources.

3.1.2. Dispersion

To analyze the dispersion of $PM_{2.5}$, PM_{10}, SO_2, and O_3, the Python (v3.10.0) software (Matplotlib) was used to create boxplot graphs as shown in Figure 3.

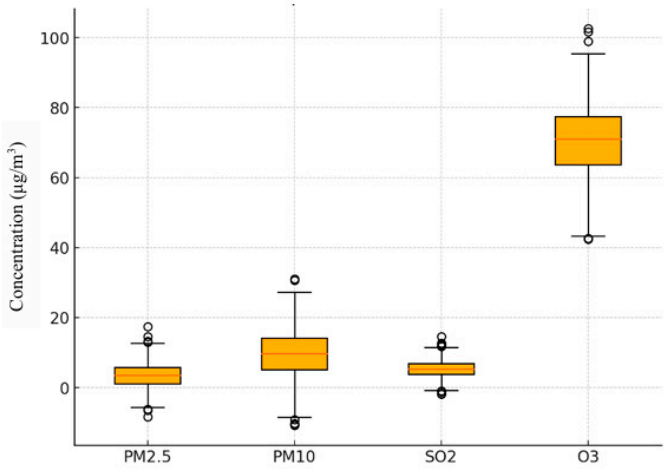

Figure 3. Boxplot for the distributions of the values of $PM_{2.5}$, PM_{10}, SO_2, and O_3.

$PM_{2.5}$ and SO_2 present distributions concentrated at low values of their concentration, with some extreme events. The concentration data from the PM_{10} series presents greater variability than the $PM_{2.5}$ series.

The statistical analysis of pollutant concentrations in 2024 reveals notable variability, particularly for O_3 and $PM_{2.5}$. O_3 concentrations have a median value of 72.1 $\mu g/m^3$ and a wide range, indicating the occurrence of high-concentration episodes. $PM_{2.5}$ values show extreme outliers, which may correspond to critical pollution events. Although only a general overview of dispersion is provided here, a detailed analysis of extreme values and outliers for $PM_{2.5}$ and PM_{10} concentrations is presented later in Sections 3.3.1 and 3.3.2, where critical pollution episodes are examined in depth.

3.1.3. Linear Trends and Coefficients of Determination

The coefficient of determination (R^2) values for the parameters analyzed are shown in the graphs in Figure 2. For $PM_{2.5}$ particles (Graph 2.1), R^2 = 0.0296, and the trend analysis suggests higher concentrations at the beginning of the year, based on the negative slope of the linear regression line fitted to the $PM_{2.5}$ time series. Although no explicit

equation is provided, a general linear trend model can be expressed as $C(t) = a \cdot t + b$, where $C(t)$ is the concentration at time t, a is the slope, and b is the intercept. The straight-line equation indicates a higher concentration at the beginning of the year. Graph 2.2 shows the concentration of PM_{10} particles, with a coefficient of determination $R^2 = 0.0244$. This graph shows variations in the concentration of particles over time, with peaks at certain times of the year. The linear trend is slightly increasing. For SO_2, the calculations show a coefficient of determination $R^2 = 0.2748$ (Graph 2.3). The initial concentration is high, followed by stabilization at lower values. The linear trend points to a slight decrease over time. Analyzing Graph 2.4, which shows the concentration of O_3 in the atmosphere throughout the year 2024, this concentration presents a very high initial peak, followed by stabilization at lower values. The trend line suggests a slight reduction in concentration over time. The coefficient of determination R^2 is equal to 0.0606.

These R^2 values indicate that linear trends (concentrations versus days of the year) explain little of the variability in the data, suggesting that other factors may significantly influence the concentration of the parameters under analysis. Therefore, 2.96%, 2.44%, 27.5%, and 6.06% of the variability of the dependent variable is explained by the independent variables included in the regression model. This indicates that the linear models have low explanatory power, suggesting that other factors not included in the regression exert a significant influence on the variability of the concentrations. Nonlinear or multivariate models may be more suitable for explaining the observed variability. Graphs 2.1 to 2.4 show distinct patterns, with some showing large spikes and others showing clearer stabilization. Most series have a slightly decreasing trend, except for Graph 2.2, where the slope of the line is positive.

3.2. Probability Distributions Modeling

3.2.1. Fitting $PM_{2.5}$ and PM_{10} Distributions

Statistical modeling of the concentration of airborne particles, such as $PM_{2.5}$ and PM_{10}, is essential to understand their variability and environmental impact. The application of appropriate statistical distributions allows the behavior of these concentrations to be accurately described, facilitating predictions, risk assessments, and the formulation of environmental policies. Statistical distributions such as Weibull, Lognormal, Normal, and Gamma are commonly employed to model natural phenomena characterized by asymmetry and variability. For example, Lu [38] used these three theoretical distributions—Lognormal, Weibull, and Pearson type V—to fit the distribution of PM_{10} concentrations at five air monitoring stations in Taiwan from 1995 to 1999.

In this study, we applied these same distributions to the particulate matter concentrations under investigation. Figure 4 illustrates the fits of the Weibull, Lognormal, Normal, and Gamma distributions to the data, highlighting the patterns in the observed concentrations. Additionally, to further clarify the fitting process, the mathematical Equations (1)–(4) for the Normal, Lognormal, Weibull, and Gamma distributions are provided below:

- *Normal Distribution:*

$$f(x) = \frac{1}{\sigma\sqrt{2\pi}}\, exp\left(-\frac{(x-\mu)^2}{2\,\sigma^2}\right) \quad (1)$$

where

μ is the mean;
σ is the standard deviation;
x is the random variable.

- *Lognormal Distribution:*

$$f(x) = \frac{1}{x\sigma\sqrt{2\pi}} \exp\left(-\frac{(ln(x)-\mu)^2}{2\sigma^2}\right), \quad x > 0, \tag{2}$$

where

μ is the mean of the natural logarithm of x;
σ is the standard deviation of the natural logarithm of x.

- *Weibull Distribution:*

$$f(x) = \frac{c}{\lambda}\left(\frac{x}{\lambda}\right)^{c-1} \exp\left(-\left(\frac{x}{\lambda}\right)^{c}\right), \quad x \geq 0 \tag{3}$$

where

$c > 0$ is the shape parameter;
$\lambda > 0$ is the scale parameter.

- *Gamma Distribution:*

$$f(x) = \frac{1}{\Gamma(\alpha)\theta^{\alpha}} x^{\alpha-1} e^{-x/\theta}, \quad x > 0, \tag{4}$$

where

$\alpha > 0$ is the shape parameter;
$\theta > 0$ is the scale parameter;
$\Gamma(\alpha)$ is the Gamma function.

These mathematical expressions accurately describe the theoretical behavior of the $PM_{2.5}$ and PM_{10} concentrations modeled in this study.

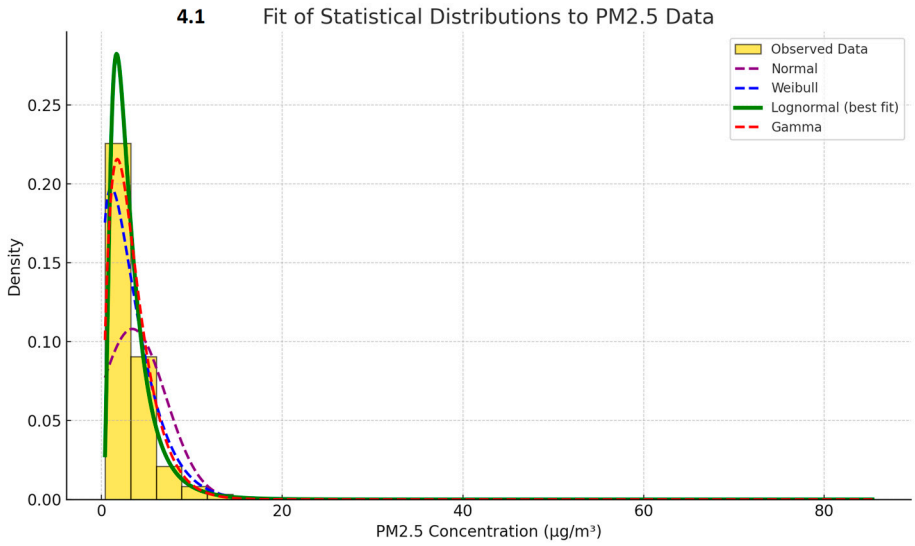

Figure 4. *Cont.*

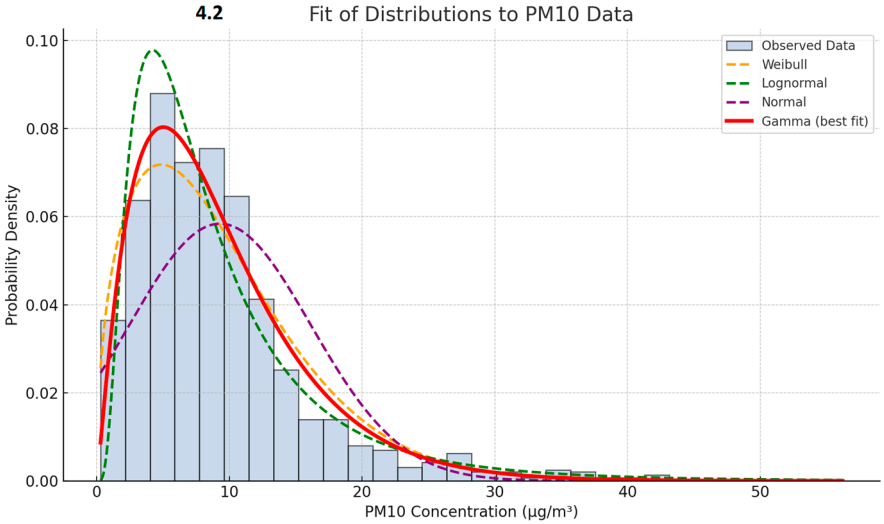

Figure 4. Adjustments of the Weibull, Lognormal, Normal, and Gamma statistical distributions, applied to $PM_{2.5}$ and PM_{10} concentrations.

Both distributions (Graphics 4.1 and 4.2) present asymmetry to the right, the PM_{10} distribution is more elongated, indicating greater variability and the presence of extreme values. The distribution of $PM_{2.5}$ is more concentrated, while PM_{10} has a longer tail. In the case of $PM_{2.5}$, the Lognormal distribution is the one that presents the best fit. PM_{10} particles present greater variability than $PM_{2.5}$, which may indicate different sources or dispersion processes in the environment. The longer tail of the PM_{10} distribution suggests that high-concentration events are more common for these particles than for $PM_{2.5}$. PM_{10} concentration tends to follow asymmetric distributions due to emission and deposition processes, in which case the distribution that best fits is Gamma. The histograms show that both distributions are skewed to the right, indicating that there is a majority of low values, with some sporadic high-concentration events. These events may be associated with intermittent sources such as dust storms or irregular industrial emissions.

As mentioned previously, to analyze the distribution pattern of $PM_{2.5}$ and PM_{10} concentrations recorded on Faial Island, four theoretical distributions were fitted to the empirical data: Normal, Weibull, Gamma, and Lognormal. Tables 2 and 3 show, respectively, the fitted parameters for the four $PM_{2.5}$ and PM_{10} distributions.

Table 2. Parameters of the theoretical distributions fitted to the observed $PM_{2.5}$ concentration data ($\mu g/m^3$). The Normal, Weibull, Lognormal, and Gamma models were applied, and their respective shape and scale parameters are reported where applicable. Mean and standard deviation values are included for comparative purposes. Symbols: μ—mean, σ—standard deviation, α—shape parameter (Gamma), θ—scale parameter (Gamma and Lognormal), c—shape parameter (Weibull), λ—scale parameter (Weibull).

	$PM_{2.5}$			
Parameters	**Mean ($\mu g/m^3$)**	**Standard Deviation ($\mu g/m^3$)**	**Shape**	**Scale**
Normal Distribution	μ = 3.43	σ = 3.69	---	---
Weibull Distribution	---	---	c = 1.27	λ = 3.74
Lognormal Distribution	---	---	σ = 0.67	θ = 2.64
Gamma Distribution	---	---	α = 2.06	θ =1.66

Table 3. Parameters of the theoretical distributions fitted to the observed PM_{10} concentration data ($\mu g/m^3$). The Normal, Weibull, Lognormal, and Gamma models were applied to the data series, and the corresponding shape and scale parameters are reported. Mean and standard deviation values are included for reference. Symbols: μ—mean, σ—standard deviation, α—shape parameter (Gamma), θ—scale parameter (Gamma and Lognormal), c—shape parameter (Weibull), λ—scale parameter (Weibull).

	PM_{10}			
Parameters	**Mean($\mu g/m^3$)**	**Standard Deviation ($\mu g/m^3$)**	**Shape**	**Scale**
Normal Distribution	$\mu = 9.3$	$\sigma = 6.83$	---	---
Weibull Distribution	---	---	$c = 1.43$	$\lambda = 10.3$
Lognormal Distribution	---	---	$\sigma = 0.74$	$\theta = 7.26$
Gamma Distribution	---	---	$\alpha = 2.18$	$\theta = 4.27$

3.2.2. Goodness-of-Fit Criteria (KS, AIC, BIC)

After it was assessed the Kolmogorov–Smirnov test, Akaike Information Criterion (AIC = $2k - 2\ln(L)$, K (number of model parameters), L (likelihood function value)) and Bayesian Information Criterion (BIC = $K \ln(n) - 2 \ln(L)$, n (number of observations)). These criteria are essential to assess the suitability of each model. Table 4 shows the results of these tests for $PM_{2.5}$ and Table 5 for PM_{10}.

Table 4. Goodness-of-fit statistics for the distribution models applied to $PM_{2.5}$ concentration data. The Kolmogorov–Smirnov (KS) statistic, corresponding *p*-values, and the Akaike (AIC) and Bayesian (BIC) Information Criteria are reported for each model. Lower KS, AIC, and BIC values indicate better model fit.

	$PM_{2.5}$			
Distribution	**KS Statistic**	***p*-Value**	**AIC**	**BIC**
Normal	0.226	0.000000	94,172.0	94,187.5
Weibull	0.128	2.07×10^{-246}	75,203.2	75,218.7
Lognormal	0.044	1.23×10^{-29}	68,725.9	68,741.5
Gamma	0.089	1.84×10^{-120}	72,812.2	72,827.7

Table 5. Goodness-of-fit statistics for the distribution models applied to PM_{10} concentration data. The Kolmogorov–Smirnov (KS) statistic, corresponding *p*-values, and the Akaike (AIC) and Bayesian (BIC) Information Criteria are shown for each model. Among the models tested, the one with the lowest values for all three criteria is considered the best fit.

	PM_{10}			
Distribution	**KS Statistic**	***p*-Value**	**AIC**	**BIC**
Normal	0.123	4.37×10^{-263}	123,842.5	123,858.1
Weibull	0.064	2.87×10^{-67}	115,423.9	115,439.6
Lognormal	0.058	4.83×10^{-55}	114,784.3	114,799.9
Gamma	0.045	1.48×10^{-33}	114,488.1	114,503.7

Among the tested models, the Lognormal distribution exhibited the best fit, showing the lowest KS statistic (0.044) and the lowest AIC (68,7259) and BIC (68,7415) values. This suggests that $PM_{2.5}$ concentrations are positively skewed and better represented on a logarithmic scale, which is consistent with findings in atmospheric pollution literature.

For PM_{10}, the quality of fit was evaluated using the KS test, along with the AIC and BIC. Among the distributions tested, the Gamma distribution exhibited the best overall performance: it had the lowest KS statistic (0.045), indicating minimal deviation between the empirical and theoretical distributions. It produced the lowest AIC (114,488) and BIC (114,504) values, confirming the best trade-off between model fit and complexity. Although all *p*-values were very small due to the large sample size, a common occurrence in environmental data, the Gamma distribution still yielded the highest *p*-value among the alternatives.

To estimate possible critical episodes of $PM_{2.5}$ the Probability Density Function (PDF) and the Cumulative Distribution Function (CDF) were calculated. These functions can be seen in Figure 5.

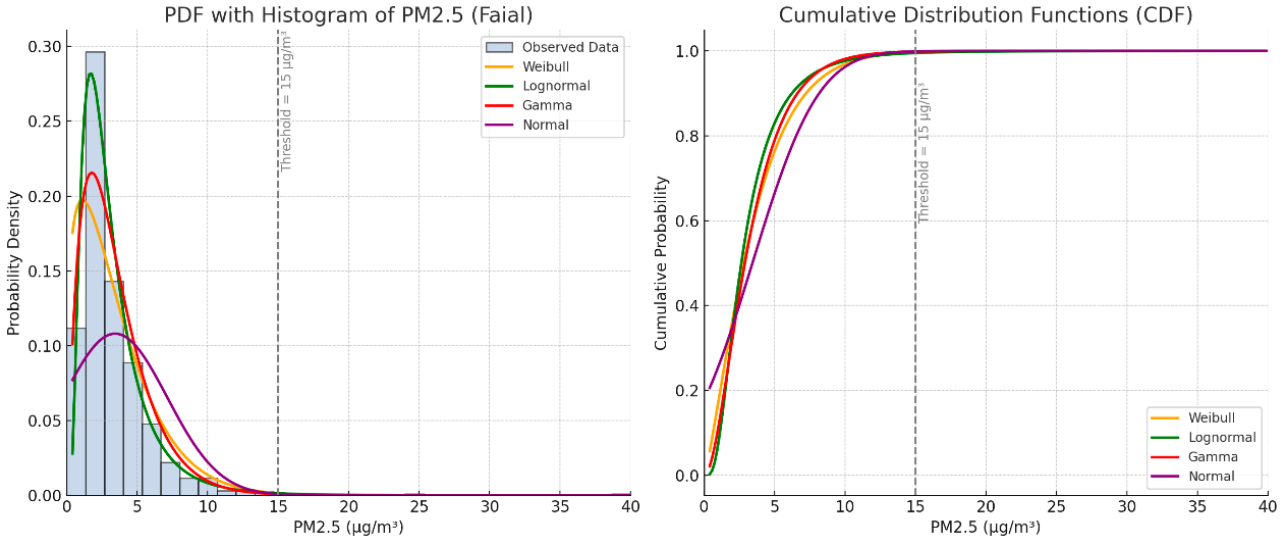

Figure 5. $PM_{2.5}$, (**Left**) PDF with histogram of observed data and fitted curves (Normal, Weibull, Lognormal, Gamma). (**Right**) Theoretical CDFs for the same distributions, showing cumulative behavior.

The histogram and PDF reveal that $PM_{2.5}$ tends to cluster between 1 and 4 $\mu g/m^3$, with a median close to 2.6 $\mu g/m^3$, below the limits harmful to health recommended by the World Health Organization (WHO). The CDF allows precise estimation of exceedance probabilities. For instance, the probability of exceeding the 15 $\mu g/m^3$ WHO daily guideline is below 0.5%, suggesting that critical pollution events are rare, but should not be entirely disregarded in risk planning. The lognormal shape implies a positively skewed distribution, meaning that while high-concentration events are infrequent, they can reach extreme values, posing episodic health and environmental risks. The same statistical treatment was applied to PM_{10}, Figure 6.

From Figure 6, the PDF analysis shows a distribution with positive asymmetry, characterized by a density peak at the lowest concentrations and a long tail on the right, where episodes of greatest pollution are concentrated. This configuration is typical of environmental phenomena influenced by multiple sources and meteorological variability, as is the case with fine particulate matter. Such characteristics make the use of symmetric models such as the normal distribution unfeasible and point to asymmetric distributions such as Weibull, Lognormal, and Gamma as more appropriate options. The CDF reinforces this observation by representing the cumulative probability of occurrence of concentrations below certain reference values. This function allows, for example, to accurately determine the probability of exceeding regulatory limits (e.g., 25 $\mu g/m^3$) useful in risk assessments and air quality management.

The statistical modeling presented above establishes a robust foundation for understanding the probabilistic behavior of $PM_{2.5}$ and PM_{10} concentrations. However, beyond general distribution patterns, it is equally critical to examine the specific instances when pollutant levels exceed regulatory thresholds. These exceedances can have significant health and environmental implications, particularly in insular contexts like the Azores. The following section investigates such critical pollution episodes, exploring their frequency, intensity, and associated meteorological conditions observed during 2024.

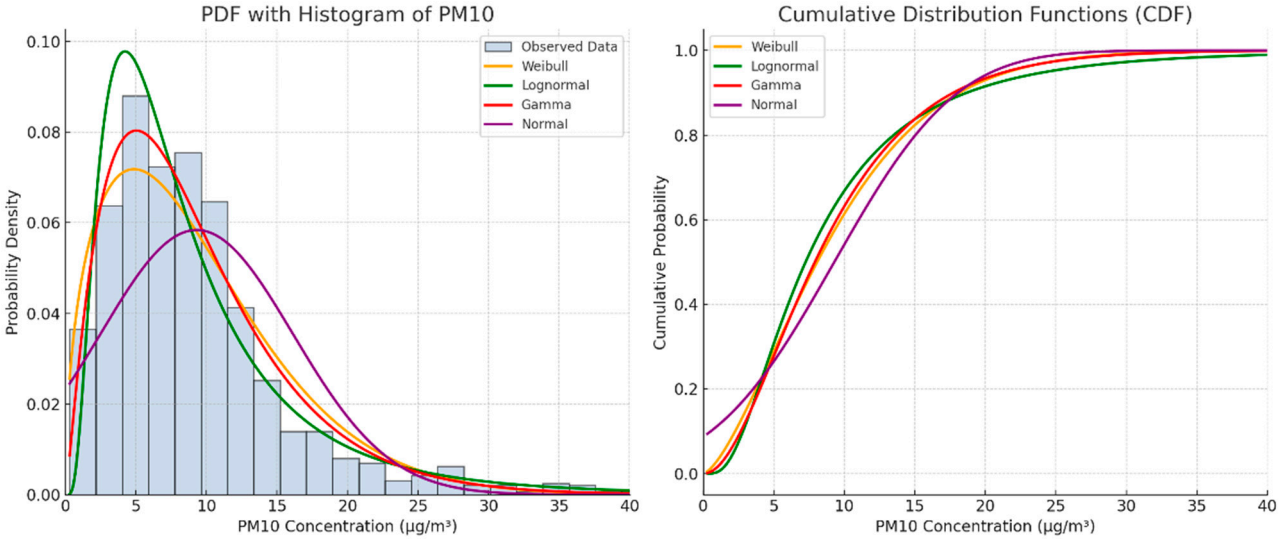

Figure 6. PM_{10}, (**Left**) PDF with histogram of observed data and fitted curves (Normal, Weibull, Lognormal, Gamma). (**Right**) Theoretical CDFs for the same distributions, showing cumulative behavior.

3.3. Exceedances: Regulatory Thresholds and Legislative Context

The Diário da República, the official gazette of Portugal, defines the upper and lower assessment thresholds for ambient air pollutant SO_2 concentrations in a zone or agglomeration for health and vegetation safety, as presented in Table 6 [39].

Table 6. Upper and lower assessment thresholds for sulfur dioxide (SO_2) concentrations, based on Portuguese and European legislation. Thresholds are defined separately for human health protection (daily average) and vegetation protection (winter average), expressed in $\mu g/m^3$ [39].

	SO_2	
	Health safety	Vegetation safety
Upper assessment threshold	60% of the limit value per twenty-four-hour period (75 $\mu g/m^3$, not to be exceeded more than three times per calendar year).	60% of the critical level applicable in winter (12 $\mu g/m^3$).
Lower assessment threshold	40% of the limit value per twenty-four-hour period (50 $\mu g/m^3$, not to be exceeded more than three times per calendar year).	40% of the critical level applicable in winter (8 $\mu g/m^3$).

Based on the reference mentioned above, Table 7 presents the upper and lower assessment thresholds for particulate matter.

Table 7. Upper and lower assessment thresholds for particulate matter ($PM_{2.5}$ and PM_{10}), as established in Portuguese and EU air quality legislation. Thresholds refer to daily and annual mean values and are expressed in $\mu g/m^3$. These thresholds guide air quality evaluation and intervention planning [39].

	$PM_{2.5}$/PM_{10}		
	Average per twenty-four-hour period (PM_{10})	Annual average $PM_{2.5}$ (1)	Annual average PM_{10}
Upper assessment threshold	70% of the limit value (35 $\mu g/m^3$, not to be exceeded more than 35 times per calendar year).	70% of the limit value (17 $\mu g/m^3$).	70% limit value (28 $\mu g/m^3$).
Lower assessment threshold	50% of the limit value (25 $\mu g/m^3$, not to be exceeded more than 35 times per calendar year).	50% of the limit value (12 $\mu g/m^3$).	50% of the limit value (20 $\mu g/m^3$).

(1) The upper assessment threshold and the lower assessment threshold for PMs do not apply to measurements made to assess the achievement of the PM exposure reduction target.

Continuing with the same legislative reference, Table 8 presents the information and alert thresholds for ozone (O_3) concentrations, as defined in Portuguese legislation [39]. These thresholds aim to inform the public and guide actions during episodes of elevated ozone levels.

Table 8. Information and alert thresholds for tropospheric ozone (O_3), defined for 1 h exposure periods. These thresholds are used to inform the public and activate health protection measures during elevated ozone episodes [39].

Objective	**Reference Period**	**Threshold**
Information	1 h	180 $\mu g/m^3$
Alert	1 h	240 $\mu g/m^3$

Similarly, Table 9 summarizes the limit values for PM_{10} concentrations established to protect human health, also based on the same official source.

Table 9. Limit values for PM_{10} concentrations set for the protection of human health. The daily and annual limit values refer to ambient air concentrations not to be exceeded more than a specified number of times per calendar year [39].

Reference Period	**Limit Value**
PM_{10}	
One day	50 $\mu g/m^3$, not to exceed 35 times per calendar year
Calendar year	40 $\mu g/m^3$

In the context of the 2024 dataset, a correlation analysis was conducted between $PM_{2.5}$ and PM_{10} concentrations (including exceedance periods) and the levels of SO_2 and O_3, with the goal of understanding their combined influence on air quality and the potential implications for public health and the environment. This analysis takes into account the threshold values established in the Portuguese Official Gazette [39], including the upper and lower assessment levels for each pollutant and the information and alert thresholds for ozone.

Before examining the specific exceedance events recorded in 2024, it is important to frame the analysis within the context of regulatory thresholds established for public health and environmental protection. The European Union and national legislation define upper and lower assessment thresholds for particulate matter ($PM_{2.5}$ and PM_{10}) and atmospheric pollutants such as SO_2 and O_3. These thresholds serve as benchmarks for triggering air quality alerts, informing risk communication, and guiding the implementation of mitigation strategies. Throughout 2024, several days registered PM_{10} concentrations that exceeded or closely approached the legal thresholds established for health protection. Notably, on 26–27 January, 2, 4, 5, and 6 February, 14–16 April, 11 November, and 27–29 December, exceedance alerts were issued by the Portuguese Environment Agency (APA). On these dates, observed concentrations reached or surpassed the 24 h average reference limit of 50 $\mu g/m^3$, or fell within the moderate to severe outlier range as defined by statistical thresholds. These episodes are discussed in detail in the following subsections, with meteorological context and dust transport patterns provided to support interpretation.

To identify anomalous pollution episodes in the 2024 time series, we applied an interquartile range (IQR)-based method for outlier detection. Specifically, **moderate outliers** were defined as values exceeding **Q3 + 1.5 × IQR** or below **Q1 − 1.5 × IQR**, while **severe outliers** were defined using the more conservative thresholds of **Q3 + 3.0 × IQR** and **Q1 − 3.0 × IQR**. This robust method was applied to the full dataset of $PM_{2.5}$ and PM_{10} concentrations. Outliers identified through this approach were further cross-validated against known atmospheric transport events (e.g., Saharan dust intrusions) and official air quality alerts issued by the Portuguese Environment Agency.

3.3.1. $PM_{2.5}$ Outliers and Episodic Peaks

To identify anomalies (extreme values), the moderate (Figure 7) and severe (Figure 8) outliers of the $PM_{2.5}$ series were calculated for the year 2024.

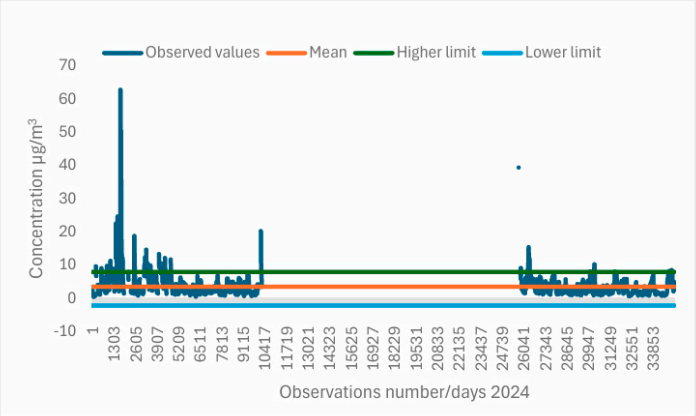

Figure 7. Moderate outliers from the $PM_{2.5}$ series for the year 2024.

The $PM_{2.5}$ time series presents 961 observed data points that are classified as moderate outliers, that is, data with values greater than 7.94 $\mu g/m^3$. And 373 observed data classified as severe outliers were detected, with data with values greater than 11.75 $\mu g/m^3$. Throughout 2024, no alerts were issued for exceedances of $PM_{2.5}$ particulate matter.

These extreme values can provide insights into anomalous patterns, highlighting the long-range transport of air masses from North Africa (Sahara), which in their composition present this type of particulate matter. On the other hand, these particles may come from forest fires in North America, Europe, or even the Amazon region and be transported to the North Atlantic, including the Azores.

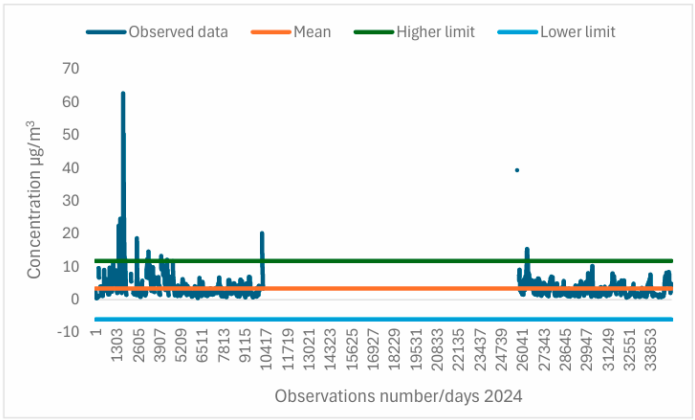

Figure 8. Severe outliers from the $PM_{2.5}$ series for the year 2024.

3.3.2. PM_{10} Outliers and Alert Periods

Moderate (Figure 9) and severe (Figure 10) outliers of the PM_{10} series for the year 2024 were calculated to identify anomalies.

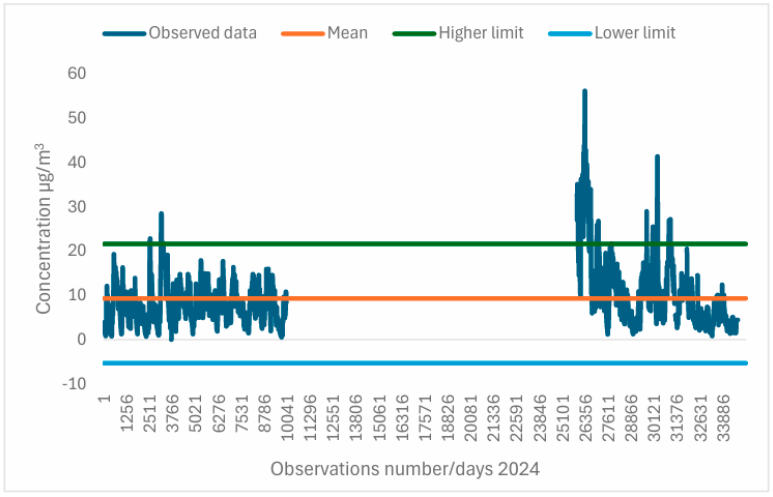

Figure 9. Moderate outliers from the PM_{10} series for the year 2024.

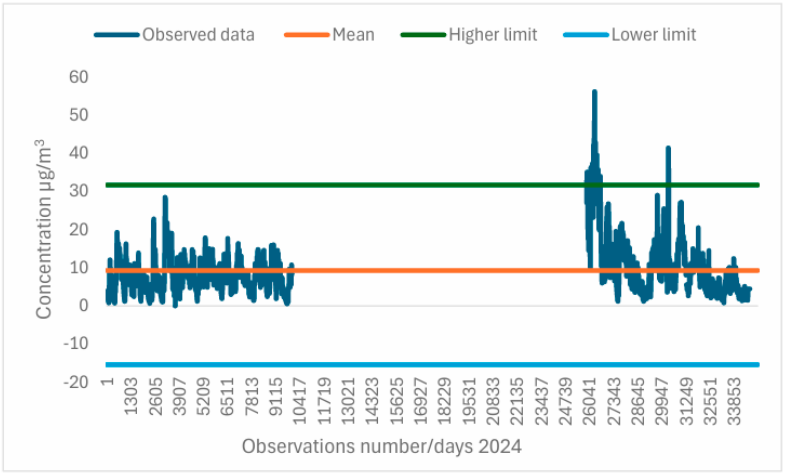

Figure 10. Severe outliers from the PM_{10} series for the year 2024.

From the analysis carried out on the PM_{10} time series (2024), 1201 data points were detected with values higher than 21.595 µg/m^3. These data are classified as moderate

outliers. Meanwhile, 314 of the observed data are severe outliers, that is, data with values greater than 31.69 $\mu g/m^3$.

Tables 10–14 summarize the synoptic conditions reported by the Portuguese Environment Agency (APA) during each PM_{10} exceedance alert. Their inclusion in the main text provides immediate access to the meteorological context, facilitating the interpretation of observed particle concentration peaks and their potential atmospheric drivers. For example, the meteorological configuration described for February 4 supports the observed PM_{10} peak of 28.2 $\mu g/m^3$, confirming the influence of Saharan dust transport on air quality in the Azores.

Table 10. Weather conditions during a PM_{10} particle alert (exceedance) event in January [40,41].

Portuguese Environment Agency (APA)—Alert Excedence PM_{10}	
Date	**Weather Conditions**
26 January 2024 to 27 January 2024	In the Azores archipelago region, a synoptic configuration conducive to the transport of suspended particles (PM10) originating from North Africa was observed. On 26 January, two anticyclonic nuclei—located over the Bay of Biscay and North Africa—interacted with a depression centered south of the archipelago, generating an easterly to southeasterly airflow in the lower levels of the troposphere. This circulation promoted the advection of air masses laden with Saharan dust, particularly over the Eastern and Central groups. Precipitation recorded in these sectors contributed to the wet deposition of particles, partially reducing atmospheric concentrations. On 27 January, the synoptic situation evolved with the establishment of an anticyclone over Central Europe, extending as a ridge toward North Africa, while a depression moved slowly northeast of the Azores. This configuration resulted in a southerly airflow over the Eastern and Central groups, rotating to a northwesterly direction throughout the day, maintaining the regime of dust transport at altitude. The occurrence of precipitation once again played a mitigating role in the levels of PM_{10} concentrations. Nevertheless, the Portuguese Environment Agency (APA) issued an alert for PM_{10} exceedance, indicating concentration levels above the recommended air quality limits for the Azores during this episode.

During the January alert period, the maximum recorded PM_{10} concentration reached 22.8 $\mu g/m^3$ over a duration of 1 h and 45 min—falling within the range classified as a moderate outlier.

A second PM_{10} exceedance alert was issued by the Portuguese Environment Agency (APA) between February 2nd and 6th. Table 11 details the meteorological conditions associated with this episode [42–45].

Table 11. Weather conditions during a PM_{10} particle alert (exceedance) event in February [42–45].

Portuguese Environment Agency (APA)—Alert Excedence PM_{10}	
Date	**Weather Conditions**
2 February 2024, 4 February 2024 and 5 February 2024, 6 February 2024	During early February 2024, multiple episodes of advection of suspended particles (PM_{10}) originating from North Africa were recorded in the Azores, driven by various large-scale synoptic configurations. On 2, 4, 5, and 6 February, the persistent presence of anticyclones located over the Iberian Peninsula, the Bay of Biscay, and North Africa, often associated with depressions to the west or northeast of the archipelago, resulted in prevailing easterly, southeasterly, and southerly airflow patterns in the lower levels of the troposphere over the Eastern and Central groups of the Azores. These atmospheric conditions favored the transport of air masses laden with desert dust at altitude, establishing a regime of natural-origin pollution. The occurrence of intermittent precipitation, particularly over the Eastern group, contributed to the attenuation of dust concentrations through wet deposition.

During the four days in February for which PM_{10} exceedance alerts were issued, the maximum particulate concentration reached 28.2 $\mu g/m^3$, sustained over a period of 6 h and 15 min—within the range of moderate outliers. Despite not reaching severe thresholds,

the recurrence and persistence of the associated synoptic pattern over multiple consecutive days underscores the region's pronounced vulnerability to Saharan dust transport events, with potential consequences for ambient air quality and public health. In April, the Azores Archipelago was again placed under alert for elevated PM_{10} levels over a three-day period. The corresponding meteorological conditions, as reported by the Portuguese Environment Agency (APA), are summarized in Table 12 [46–48].

Table 12. Weather conditions during a PM_{10} particle alert (exceedance) event in April [46–48].

Portuguese Environment Agency (APA)—Alert Excedence PM_{10}	
Date	**Weather Conditions**
14 April 2024 to 16 April 2024	Between April 14 and 16, 2024, the Azores Archipelago was affected by a prolonged Saharan dust intrusion event, driven by persistent synoptic conditions favorable to the transport of suspended particulate matter (PM10) from North Africa. On 14 April, the presence of a slow-moving anticyclone west of the Azores and an upper-level depression centered west of Madeira induced an easterly airflow over the Eastern and Central groups of the Azores at low atmospheric levels, promoting dust advection at altitude. Precipitation recorded over the archipelago contributed to wet deposition, partially mitigating the impact, with estimated PM_{10} concentrations ranging between 5 and 20 $\mu g/m^3$ in the affected islands. On 15 April, favorable circulation persisted, with easterly winds over the Western and Central groups and southeasterly winds over the Eastern group. This synoptic configuration continued to support the intrusion of desert particles, with estimated PM_{10} concentrations ranging from 5 to 20 $\mu g/m^3$ in the Western and Central groups, and 20 to 50 $\mu g/m^3$ in the Eastern group. By 16 April, the anticyclone had shifted toward the west of the British Isles, while the associated depression moved slowly south of the Azores. This resulted in easterly flow over the Central group and southeasterly flow over the Eastern group, initiating the gradual displacement of the dust-laden air mass. Despite continued precipitation, PM_{10} concentrations remained elevated, with estimates between 5 and 20 $\mu g/m^3$. Forecast models indicated the dissipation of the intrusion event on the following day.

Between 14 and 16 April, the Azores experienced a Saharan dust intrusion event, driven by specific synoptic conditions that facilitated long-range atmospheric transport from North Africa. Although the episode led to elevated PM_{10} concentrations, its impact was partially mitigated by precipitation, which contributed to the removal of particulates from the atmosphere.

Later in the year, on November 11, the Portuguese Environment Agency (APA) issued another PM10 exceedance alert affecting air quality in the Azores. The meteorological context of this event is detailed in Table 13 [49].

Table 13. Weather conditions during a PM_{10} particle alert (exceedance) event in November [49].

Portuguese Environment Agency (APA)—Alert Excedence PM_{10}	
Date	**Weather Conditions**
11 November 2024	On 11 November 2024, the Azores Archipelago was under the influence of a synoptic configuration dominated by an anticyclone centered over the British Isles, extending as a ridge toward the Madeira region. This pattern resulted in a southeasterly airflow in the lower levels of the troposphere, promoting the advection of air masses containing suspended particulate matter (PM_{10}) originating from the deserts of North Africa. Precipitation over the Western and Central Island groups contributed to the wet deposition of dust particles, partially mitigating atmospheric concentrations. Estimates from the Portuguese Environment Agency (APA) indicated an increase in PM_{10} concentrations ranging from 5 to 20 $\mu g/m^3$ due to this dust intrusion event. Forecast models for dust transport and dispersion suggested the dissipation of the event on the following day, as the dust-laden air mass moved away from the region.

On 11 November 2024, the Azores were once again impacted by a Saharan dust intrusion, facilitated by a southeasterly atmospheric circulation pattern. This event led to elevated PM_{10} concentrations, though partially attenuated by precipitation. On that day, the population was exposed for a period of 3 h to a PM_{10} concentration of 41.4 $\mu g/m^3$—a value classified as a severe outlier.

A subsequent PM_{10} exceedance episode occurred between 27 and 29 December 2024. The associated meteorological conditions are summarized in Table 14 [50–52].

Table 14. Weather conditions during a PM_{10} particle alert (exceedance) event in December [50–52].

Portuguese Environment Agency (APA)—Alert Excedence PM_{10}	
Date	**Weather Conditions**
27 December 2024 to 29 December 2024	Between 27 and 29 December 2024, the Azores Archipelago was affected by a Saharan dust intrusion event, sustained by a synoptic configuration favorable to the long-range transport of suspended particulate matter (PM_{10}) at altitude. On 27 December, the presence of an anticyclone centered over Central Europe, extending as a ridge toward the Azores and North Africa, generated a southeasterly flow over the Central and Eastern groups, promoting the advection of Saharan air masses. Precipitation over the Central group contributed to attenuating PM_{10} concentrations, which were estimated to range between 5 and 20 $\mu g/m^3$. On 28 and 29 December, the anticyclone shifted northwest of the Iberian Peninsula, maintaining a ridge toward Madeira. This configuration resulted in southeasterly winds over the Central and Western groups, and easterly winds over the Eastern group, sustaining the dust transport over the archipelago. On both days, precipitation in the Western group partially mitigated particle concentrations; however, PM_{10} levels remained within the 5 to 20 $\mu g/m^3$ range across the region.

Projections from atmospheric dispersion models suggested that the episode would persist in the following days, emphasizing the prolonged nature of the favorable meteorological conditions for particle intrusion during this period.

While the preceding analyses have focused on numerical exceedance data and their temporal occurrence, visualizing the spatial dispersion of particulate matter is essential to fully understand the dynamics of pollution transport. Spatial forecast maps not only validate the occurrence of exceedance events but also contextualize them within broader atmospheric circulation patterns. This is particularly relevant in the case of Saharan dust intrusions, which affect multiple regions simultaneously. The following section presents surface dust concentration forecasts, providing visual confirmation of the long-range transport mechanisms that influenced air quality episodes in the Azores during 2024.

3.3.3. Saharan Dust Surface Forecast Maps

Dust transport forecast maps for arid regions, depicting surface particle concentrations at 0, 6, 12, and 18 UTC, are available from the Copernicus Atmosphere Monitoring Service (CAMS) and the University of Athens. Figure 11, presented below, compiles a series of maps corresponding to key PM_{10} exceedance periods recorded in the Azores during 2024. These visualizations provide compelling evidence supporting the hypothesis that extreme PM_{10} events observed at the Espalhafatos station were driven by long-range Saharan dust transport. The maps reveal elevated dust concentrations reaching the Northeast Atlantic, including the Azores archipelago, and align temporally with alert days issued by the Portuguese Environment Agency (APA). This spatial and temporal correspondence reinforces the physical interpretation of the exceedance episodes and underscores the transboundary nature of particulate matter pollution, particularly in insular and remote regions. By visually linking pollution events to synoptic-scale atmospheric transport,

Figure 11 highlights the critical need for integrated monitoring and forecasting systems that account for both local emissions and distant aerosol sources.

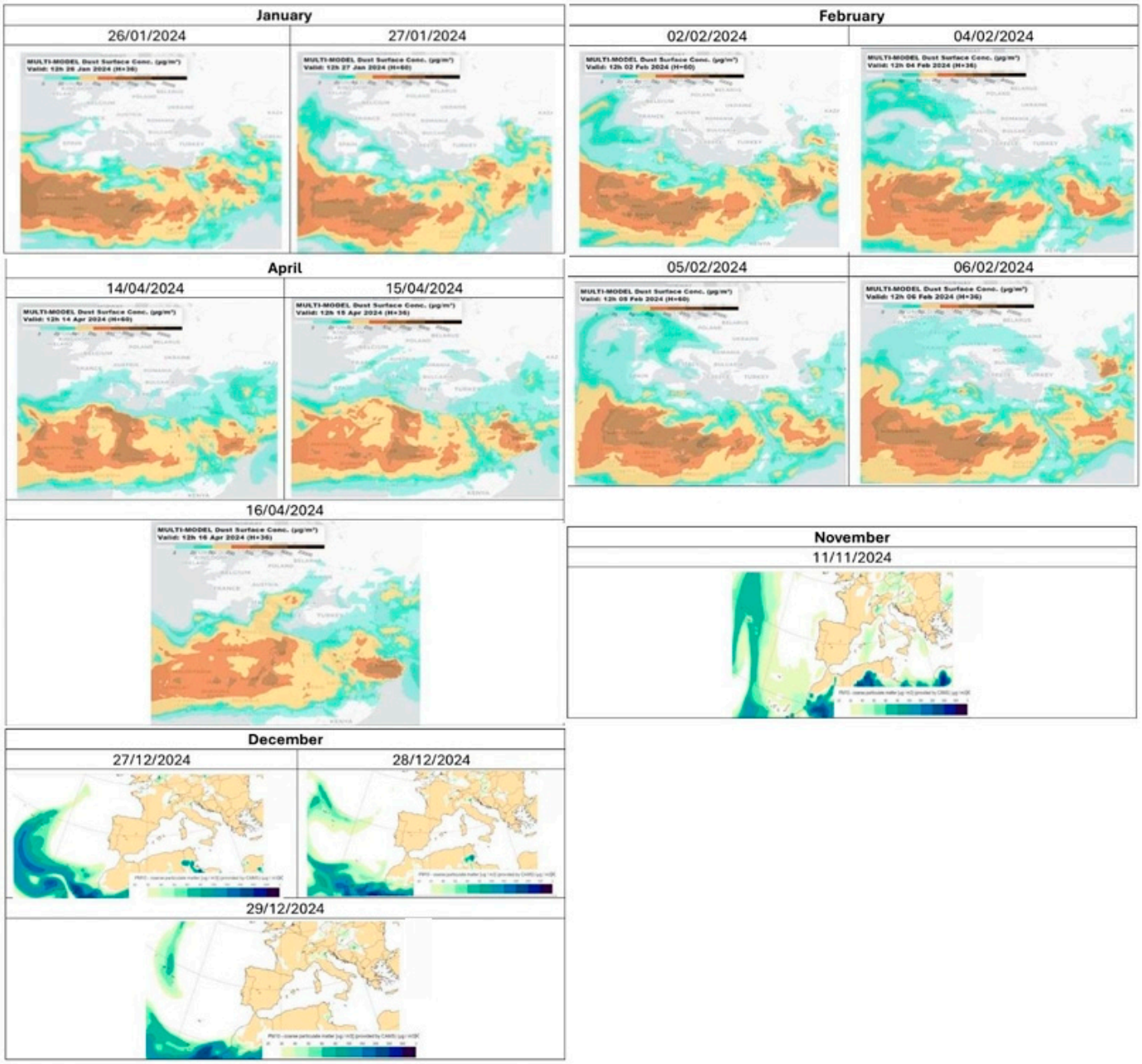

Figure 11. Forecast maps of dust surface concentration ($\mu g/m^3$) during alert periods over the Azores in 2024. The maps correspond to dates when exceedance events were identified or confirmed by the Portuguese Environment Agency (APA), spanning January, February, April, November, and December. Forecasts are based on multi-model outputs (e.g., CAMS and SKIRON) and illustrate the horizontal dispersion of mineral dust transported from North Africa toward the Northeast Atlantic. Each panel displays the predicted distribution of surface dust for a specific day, with color gradients representing concentration levels from 10 to 5000 $\mu g/m^3$. Episodes shown include the following: 26–27 January, 2, 4–6 February, 14–16 April, 11 November, and 27–29 December [40–52].

While the CAMS and SKIRON forecasts provide valuable support in identifying potential Saharan dust intrusions, their outputs should be interpreted with caution. These models operate at synoptic scales and may not fully capture the spatial complexity or local deposition processes over small islands like Faial. The absence of direct satellite valida-

tion against local PM_{10} measurements further limits their standalone diagnostic power. Nevertheless, when combined with in situ observations, they offer a useful framework for understanding regional transport mechanisms.

The regions most affected by dust transport included much of southern Europe, namely Spain, France, Italy, and Greece, as well as the Eastern Mediterranean. Notably, during the episodes of November and December, a significant dispersion of dust toward the Northeast Atlantic was also observed, clearly encompassing the Azores region. This pattern confirms that Saharan dust transport is not restricted to the European continent but extends to insular areas of the Atlantic. These findings underscore the importance of incorporating such remote territories into atmospheric monitoring networks and environmental impact assessments.

Beyond the identification of exceedance events and their synoptic drivers, it is essential to understand how different atmospheric pollutants interact with one another and respond to meteorological conditions. Such interactions can reveal potential common sources, secondary formation processes, and environmental feedback mechanisms that influence pollutant dynamics. In insular and meteorologically complex regions like the Azores, these relationships are often nonlinear and sensitive to temporal lags. The following section explores the statistical correlations and time-lagged dependencies between particulate matter ($PM_{2.5}$ and PM_{10}), sulfur dioxide (SO_2), and ozone (O_3), aiming to uncover patterns that may inform predictive modeling and public health risk assessments.

3.4. Correlation and Time Lag Analysis

3.4.1. PM vs. SO_2 and O_3

An analysis of the correlations between $PM_{2.5}$, PM_{10}, SO_2, and O_3 was conducted using hourly data from 2024, with a consistent dataset containing 20,265 simultaneous observations for all variables. Pearson and Spearman coefficients were used to assess relationships. In Figure 12, the results reveal distinct interaction patterns among these parameters.

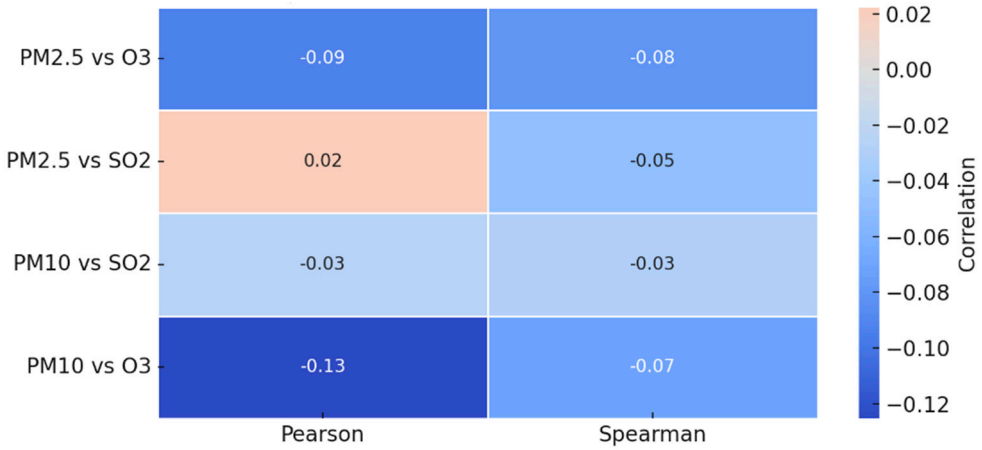

Figure 12. Heatmap of correlations (Pearson and Spearman coefficients) between $PM_{2.5}$, PM_{10}, O_3, and SO_2.

The correlation between $PM_{2.5}$ and O_3 was weak and negative (Pearson = −0.093; Spearman = −0.081), suggesting a slight tendency for ozone levels to decrease when fine particulate concentrations increase. This may be due to reduced solar radiation available for ozone formation in polluted conditions. The relationship between $PM_{2.5}$ and SO_2 was extremely weak (Pearson = +0.022; Spearman = −0.048), indicating virtually no direct association. While SO_2 can contribute to secondary aerosol formation, this effect was not evident in the data. The correlation between PM_{10} and SO_2 was similarly weak and

negative (Pearson = −0.026; Spearman = −0.030), suggesting that even if these pollutants share sources like combustion, they did not exhibit synchronous patterns. The strongest relationship was observed between PM_{10} and O_3, with a moderate negative correlation (Pearson = −0.125). This supports the hypothesis that higher concentrations of coarse particles may reduce the formation of ozone by attenuating solar radiation or altering photochemical reactions.

To better understand the behavior of O_3 in the study area, we examined its diurnal variability across the available months. As expected, concentrations exhibited a characteristic daily cycle, with peaks during early afternoon hours and troughs during the night, consistent with the influence of solar radiation on ozone photochemistry. This reinforces the need to interpret average O_3 values within the context of temporal dynamics.

3.4.2. Time-Lagged Regression: SO_2 and O_3

The correlation analysis between ozone (O_3) and sulfur dioxide (SO_2) concentrations revealed a positive and statistically meaningful association. The Pearson correlation coefficient was 0.237, indicating a moderate linear relationship, while the Spearman coefficient was slightly higher at 0.289, suggesting a somewhat stronger monotonic trend (Table 15).

Table 15. Correlations (Pearson and Spearman coefficients) between O_3 and SO_2.

Method	Correlation
Pearson	0.237
Spearman	0.289

These results indicate that increases in SO_2 concentrations are generally accompanied by increases in O_3 levels, albeit with a modest strength of association. This correlation may reflect the influence of common emission sources—such as urban combustion processes—or the effect of shared meteorological drivers, including ambient temperature, solar radiation intensity, and boundary layer dynamics. Nevertheless, it is important to emphasize that correlation does not imply causation.

To explore the temporal association between SO_2 and ozone O_3, a simple linear regression model was employed as shown in Equation (5), in which SO_2 values were lagged by +3 h—the time shift that maximized the Pearson correlation between the two variables. The model aimed to evaluate whether past SO_2 levels could help explain subsequent variations in O_3 concentrations. The regression was specified as follows:

$$O_3(t) = \beta_0 + \beta_1 \cdot SO_2(t - \Delta t) + \varepsilon \quad (5)$$

where

- $O_3(t)$ is the observed ozone concentration at time t;
- $SO_2(t - \Delta t)$ is sulfur dioxide concentration measured at a previous time $(t - \Delta t)$(with a time lag Δt, e.g., 3 h);
- β_0 is the intercept of the regression line (value of O_3 when SO_2 is zero);
- β_1 is the regression coefficient (slope) indicating how much O_3 changes per unit change in lagged SO_2;
- ε is the random error term (residuals) capturing the variation not explained by the model.

The model yielded a statistically significant positive relationship ($\beta_1 = 1.005$, $p < 0.001$), indicating that higher SO_2 levels tend to precede increases in O_3. However, the coefficient of determination ($R^2 = 0.056$) indicates that SO_2 alone accounts for just 5.6% of the variability in O_3 concentrations, Figure 13.

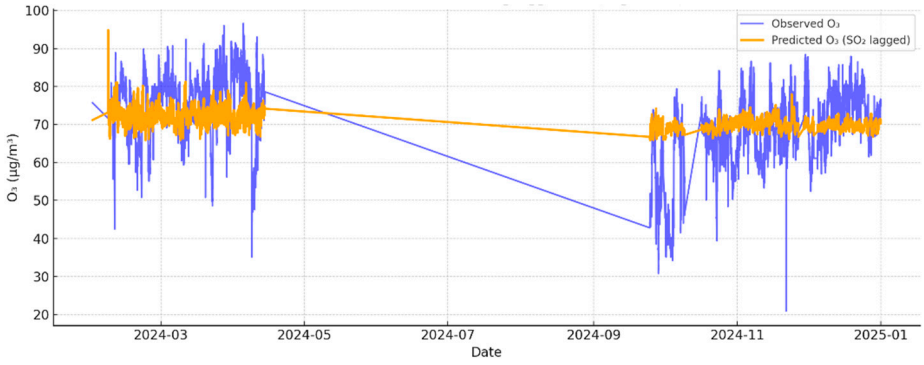

Figure 13. Observed versus predicted O_3 using lagged SO_2 (lag = +3h).

Despite the statistical significance of the regression, the low R^2 value (5.6%) indicates that the model explains only a small portion of the variability in ozone concentrations. This suggests caution in interpreting SO_2 as a strong predictor of O_3 levels, as other environmental and chemical factors are likely dominant.

This finding implies that, although SO_2 may be weakly associated with ozone formation or accumulation under certain atmospheric conditions, additional factors, particularly meteorological variables, and photochemical precursors, are likely to play a dominant role.

Although the time-lagged regression yielded statistically significant results, a more technical explanation is warranted. The rationale for exploring a +3 h lag between SO_2 and O_3 is grounded in the fact that ozone is not emitted directly but forms through secondary photochemical reactions, often involving SO_2 and other precursors such as nitrogen oxides (NO_x) and volatile organic compounds (VOCs). These reactions are sensitive to solar radiation and temperature, with delays of several hours being typical in clean or insular environments. The optimal lag was determined through a preliminary cross-correlation analysis, selecting the time interval that maximized the Pearson correlation coefficient. This approach is exploratory and consistent with prior studies on delayed pollutant interactions. Nonetheless, we acknowledge that ozone formation involves nonlinear processes, and future work will benefit from multivariate or process-based models.

3.4.3. Time-Lagged Regression: SO_2 and $PM_{2.5}$

To explore the potential temporal association between sulfur dioxide (SO_2) and fine particulate matter ($PM_{2.5}$), a simple linear regression model was constructed, as shown in Equation (6). In this analysis, the $PM_{2.5}$ time series lagged by 6 h, which corresponded to the time shift yielding the highest absolute Pearson correlation with SO_2 concentrations.

The model assumes that variations in earlier $PM_{2.5}$ levels may help explain subsequent changes in SO_2 concentrations. Mathematically, the relationship is described as follows:

$$SO_2(t) = \beta_0 + \beta_1 \cdot PM_{2.5}(t - \Delta t) + \varepsilon \quad (6)$$

where

- $SO_2(t)$ is the sulfur dioxide concentration at time t;
- $PM_{2.5}(t - \Delta t)$ is the concentration of fine particulate matter at a previous time $(t - \Delta t)$ (in this case, 6 h);
- β_0 is the intercept;
- β_1 is the slope coefficient representing the change in SO_2 per unit change in lagged $PM_{2.5}$;
- ε is the error term accounting for unexplained variability.

In this study, the optimal time lag was determined to be six hours. The model aimed to assess whether future $PM_{2.5}$ concentrations could reflect past levels of SO_2 (Figure 14), possibly due to shared sources or secondary aerosol formation.

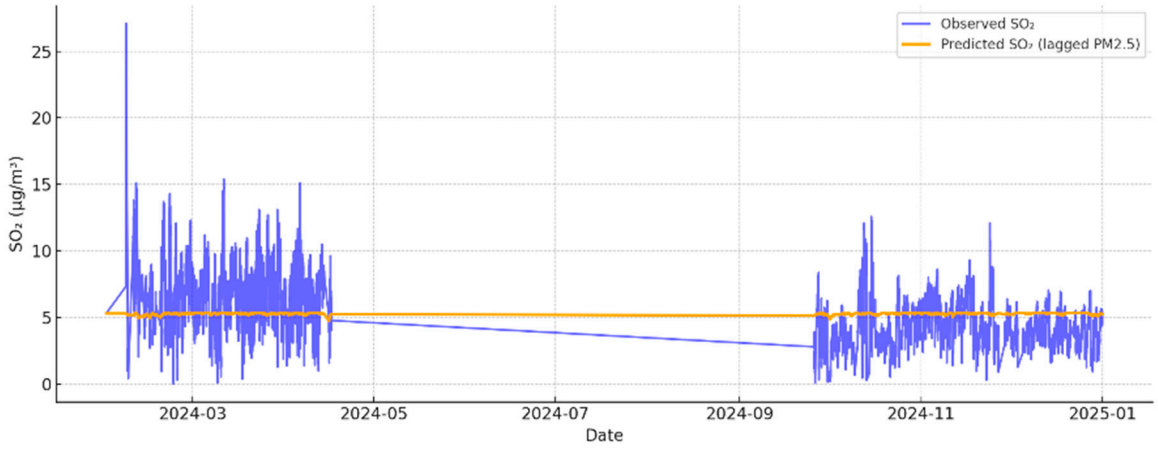

Figure 14. Observed versus predicted SO_2 using lagged $PM_{2.5}$ (lag = −6h).

The resulting model was statistically significant ($p < 0.001$), with a negative regression coefficient of −0.033. This suggests that higher $PM_{2.5}$ levels, occurring approximately six hours after SO_2, are associated with a slight decrease in SO_2 concentrations. However, the explained variance was extremely low ($R^2 = 0.002$), indicating that the model accounts for only 0.2% of the variability in SO_2 levels.

Although statistically significant, the model's explanatory power is extremely limited ($R^2 = 0.2\%$), which implies that SO_2 has almost no predictive value for $PM_{2.5}$ concentrations in this dataset. The observed association may reflect background variability or coincidental trends. Future models should consider nonlinear and multivariate approaches to better capture these complex atmospheric interactions.

4. Discussions

Due to significant data gaps between April and September, the results presented here are not intended to capture full seasonal patterns. Instead, the study emphasizes episodic events with confirmed air quality exceedances.

4.1. Interpretation of Statistical Distributions

The statistical distribution fitting conducted in this study revealed clear asymmetry in the behavior of atmospheric particulate matter concentrations observed over Faial Island. $PM_{2.5}$ concentrations were best described by a Lognormal distribution. This finding aligns with Zhang et al. [35], who demonstrated that the lognormal distribution more accurately represents the global distribution of $PM_{2.5}$ concentrations compared to the Normal distribution. Similarly, while PM_{10} concentrations were more accurately modeled using a Gamma distribution in this study, Noor et al. [36] reported that the Gamma distribution provided the best fit for PM_{10} observations in Nilai, whereas the Lognormal distribution was more appropriate for Shah Alam.

This distinction between the optimal distributions for $PM_{2.5}$ and PM_{10} is meaningful both statistically—highlighting the differing shapes and tail behaviors of the fitted models—and physically, as it reflects the contrasting emission sources, atmospheric behaviors, and transport mechanisms associated with fine and coarse particulate matter.

The suitability of the Lognormal distribution for $PM_{2.5}$ reflects the influence of multiple low-magnitude sources and the occasional presence of high-intensity events. Lognormal

behavior is typically associated with secondary particulate formation, combustion emissions, and pollutant accumulation under stable atmospheric conditions. The right-skewed nature of the distribution implies that, although most concentrations remain low, sporadic episodes of substantially elevated values may occur. These rare but critical peaks carry important environmental and health implications, reinforcing the need for robust air quality monitoring systems.

In contrast, the Gamma distribution was found to provide the best fit for PM_{10} concentrations. This distribution is frequently observed in datasets influenced by natural dust events, such as those originating from the Sahara. The heavier tail and broader spread of the PM_{10} distribution reflect greater variability, consistent with the episodic nature of dust intrusions that affected the Azores throughout 2024. The Gamma model's capacity to capture this behavior is crucial for reliably estimating exceedance probabilities, especially under synoptic-scale conditions favorable to long-range dust transport.

Moreover, the use of goodness-of-fit metrics such as the Kolmogorov–Smirnov test, Akaike Information Criterion (AIC), and Bayesian Information Criterion (BIC) confirmed the adequacy of these asymmetric distributions for environmental data modeling. Their superior statistical performance relative to the Normal distribution underscores the importance of selecting probability functions that reflect the empirical characteristics of particulate matter concentrations.

Overall, the application of Lognormal and Gamma models enhances not only the statistical accuracy of concentration estimates but also the foundation for probabilistic risk assessments and air quality forecasting. These models can support the development of early warning systems and environmental policy frameworks aimed at protecting public health, particularly in vulnerable insular regions such as the Azores.

These distributional patterns are not purely statistical but reflect fundamental differences in atmospheric behavior. The Lognormal distribution fitted for $PM_{2.5}$ suggests that its formation and dispersion are governed by multiplicative processes, such as those involved in secondary aerosol production and atmospheric transformation under stable conditions. In contrast, the Gramma distribution observed for PM_{10} concentrations is consistent with episodic and additive processes, capturing the stochastic nature of natural dust intrusions and short-lived emission events. These characteristics emphasize the importance of selecting distributions that accurately reflect the physical generation and transport mechanisms of each particulate matter type.

4.2. Saharan Dust Transport Influence

The episodic peaks observed in PM_{10} concentrations are closely aligned with documented Saharan dust intrusion events, notably during November and December 2024, as demonstrated in Figure 11. These maps confirm that air masses carrying high concentrations of mineral dust frequently reach the Azores from North Africa. This reinforces the transboundary character of particulate pollution in the region, with potential implications for public health and ecosystem integrity. This highlights the importance of integrating satellite-based dust transport models into local air quality forecasting systems and supports the development of early warning mechanisms tailored to island territories, which are often underrepresented in continental-scale environmental monitoring and policy frameworks.

4.3. Significance of Weak Correlations

The weak correlations observed between atmospheric particulate matter ($PM_{2.5}$ and PM_{10}) and trace gases (SO_2 and O_3) are not anomalous in environmental studies; rather, they reflect the multifactorial nature of atmospheric chemistry and transport mechanisms in insular environments such as the Azores. Although statistically significant relation-

ships were identified such as the positive time-lagged association between SO_2 and O_3 (Pearson = 0.237, Spearman = 0.289) the low coefficients of determination (R^2 = 0.056 for O_3 predicted by lagged SO_2, and R^2 = 0.002 for SO_2 predicted by lagged $PM_{2.5}$) underscore the limited explanatory power of these simple linear models.

The weak negative correlation observed between $PM_{2.5}$ and O_3 (Pearson = −0.093) is consistent with findings reported in other studies of regional and urban air quality. Several mechanisms in the atmospheric chemistry literature explain this pattern. First, increased $PM_{2.5}$ levels can reduce the amount of solar radiation reaching the lower atmosphere, thereby limiting the photochemical production of ozone. Second, fine particles can act as surfaces for heterogeneous reactions that scavenge ozone or interfere with its formation by interacting with NO_x or VOCs. Third, ozone may be suppressed in regions with high secondary particulate formation due to precursor competition. These dynamics have been observed in studies such as [27] in Eastern China. These findings reinforce the conclusion that correlations between ozone and particulate matter are often weak or nonlinear, shaped by complex and location-specific processes.

Several factors contribute to the weakness of these correlations. First, the atmospheric formation and removal of both particulate matter and trace gases are governed by complex nonlinear processes, including photochemical reactions, secondary aerosol formation, vertical mixing, and heterogeneous chemistry. For example, ozone formation is influenced by solar radiation, temperature, volatile organic compounds (VOCs), and nitrogen oxides (NO_x), variables that were not directly included in the statistical models of this study. Likewise, $PM_{2.5}$ and PM_{10} are derived from both primary emissions and secondary transformation pathways, which can involve interactions with sulfur compounds, ammonia, and other precursors under varying meteorological conditions.

Second, the use of 15 min to hourly resolution data over an annual period introduces significant variability and potential noise, which, while useful for identifying peak events and temporal dynamics, may dilute consistent patterns of covariation over longer timescales. The large proportion of missing data, up to 57% in the case of SO_2, further limits the robustness of time-resolved statistical associations, particularly when assessing lagged effects.

Third, the orographic and meteorological complexity of the Azores contributes to highly variable boundary layer dynamics, which can decouple surface-level pollutant concentrations from regional transport patterns or emission sources. The archipelago's location in the path of subtropical anticyclones and mid-latitude cyclones generates rapidly shifting wind regimes, humidity profiles, and precipitation events, all of which modulate the dispersion, deposition, and transformation of pollutants.

Nonetheless, the detection of statistically significant albeit weak correlations is not without scientific relevance. It highlights the partial and intermittent role of co-emitted pollutants and shared atmospheric conditions while pointing to the necessity for more sophisticated modeling approaches. Multivariate and nonlinear models such as Generalized Additive Models (GAMs), machine learning algorithms, or coupled chemical-transport models may better capture the intricate interplay among meteorology, emission sources, and chemical transformations.

In this context, the findings support the hypothesis that no single pollutant or meteorological parameter can fully account for the variability in ambient air quality in the Azores. Rather, pollutant behavior is the result of complex interactions across spatial and temporal scales. Recognizing the limitations of bivariate correlation and linear regression methods is essential not only for accurate interpretation but also for guiding the development of predictive models and public health frameworks suited to island environments.

It is important to note that the regression and correlation analyses involving SO_2 were based on a reduced subset of complete hourly observations (n = 20,265), due to the exclusion of all records with missing values. This complete-case approach was adopted to avoid introducing artificial variance through imputation. However, the large proportion of missing data for SO_2 (~57.6%) may limit the statistical power and introduce potential selection bias. Although beyond the scope of this study, future analyses should explore the application of robust imputation techniques and conduct sensitivity tests to assess how the missing data treatment influences the results.

The use of aggregated O_3 values in preliminary regressions may obscure important short-term dynamics. Future analyses should incorporate process-based or hourly models to better capture photochemical patterns.

4.4. Public Health and Environmental Implications

The physical–statistical characterization of PM_{10} and $PM_{2.5}$ concentrations over Faial Island reveals patterns with significant implications for public health and environmental management, particularly in insular regions with limited adaptive capacity. Although average pollutant concentrations remained below international thresholds for much of the year, the identification of episodic exceedances, especially of PM_{10} during documented Saharan dust events, raises concerns regarding acute and cumulative exposure risks for vulnerable populations.

From a public health perspective, fine ($PM_{2.5}$) and coarse (PM_{10}) particulate matter have well-documented associations with respiratory and cardiovascular diseases, as noted in both epidemiological and toxicological literature. The right-skewed distributions identified in this study, with long tails capturing extreme concentration events, imply that even in regions characterized by generally clean air, infrequent but intense pollution episodes may disproportionately impact population health. Such episodes can exacerbate pre-existing conditions (e.g., asthma, chronic obstructive pulmonary disease, ischemic heart disease) and increase hospital admissions, particularly among children, the elderly, and individuals with comorbidities.

Moreover, the observed weak but statistically significant correlations between trace gases (SO_2 and O_3) and particulate matter concentrations suggest potential synergistic effects, whereby combined exposure to multiple pollutants under specific meteorological conditions may amplify adverse health outcomes. Although the explanatory power of these correlations is low, they underscore the need to consider pollutant mixtures rather than individual components in the design of public health alerts and exposure guidelines.

In environmental terms, the recurrent long-range transport of Saharan dust to the Azores underscores the transboundary nature of air pollution. These events are capable not only of elevating PM_{10} concentrations but also of altering nutrient dynamics in terrestrial and marine ecosystems through the deposition of mineral particles rich in iron, phosphorus, and other elements. The presence of anthropogenic components mixed with desert dust such as heavy metals or persistent organic pollutants may further amplify ecological risks, particularly in fragile island habitats.

Given the archipelago's geographic isolation, the detection and communication of these events face unique logistical challenges. The findings of this study highlight the necessity of maintaining and expanding high-frequency air quality monitoring networks, coupled with early warning systems that integrate satellite data, atmospheric transport models, and real-time sensor information. Such tools are critical not only for timely public health interventions but also for assessing long-term environmental impacts and informing land use, tourism, and agricultural policies.

Ultimately, the results support the prioritization of adaptive air quality management strategies tailored to the specific vulnerabilities of island territories. Public health agencies should consider the implementation of dynamic risk communication protocols that account for episodic pollution surges and their potential health effects, even when annual averages remain within regulatory limits. This is particularly relevant in the context of climate change, which may intensify dust storm frequency and alter transport pathways, further increasing the exposure risk in Atlantic islands like the Azores.

5. Conclusions

This study offers a comprehensive physical–statistical characterization of $PM_{2.5}$ and PM_{10} concentrations over Faial Island (Azores) throughout 2024, representing one of the most detailed analyses conducted in a remote North Atlantic insular environment. The results confirm that fine particulate matter ($PM_{2.5}$) is best modeled by a Lognormal distribution, while coarse particulate matter (PM_{10}) aligns more closely with a Gamma distribution. These distributional patterns are not merely statistical but reflect distinct physical and atmospheric processes underlying the formation, transport, and removal of these pollutants.

The heavy-tailed, right-skewed behavior observed in both distributions underscores the episodic nature of extreme pollution events, particularly during Saharan dust intrusions. These events, validated through satellite-based models (CAMS and SKIRON) and supported by meteorological reports from the Portuguese Environment Agency (APA), emphasize the transboundary nature of particulate pollution and its potential to affect even distant island regions.

From a methodological standpoint, the application of multiple distribution fitting techniques, in conjunction with Kolmogorov–Smirnov tests, AIC, and BIC criteria, highlights the importance of selecting appropriate probabilistic models for air quality assessment. These approaches enhance the robustness of exceedance estimation and support the development of risk-based frameworks for public health protection.

It is important to note that, due to significant data gaps between April and September, this study does not aim to represent seasonal variability. Rather, it provides a focused analysis of short-term pollution exceedances with confirmed environmental relevance.

While statistically significant correlations were found between SO_2 and O_3 (with a +3 h lag), and between SO_2 and $PM_{2.5}$ (with a -6 h lag), the low explanatory power of these linear models (R^2 = 5.6% and R^2 = 0.2%, respectively) suggests that simple bivariate analyses are insufficient to capture the complexity of atmospheric interactions in this region. Future studies should explore nonlinear and multivariate models incorporating meteorological and chemical variables to better understand pollutant behavior.

The public health implications are substantial. Even though average pollutant levels generally remained below international thresholds, episodic exceedances, particularly of PM_{10}, pose acute risks to vulnerable populations. These findings reinforce the need for early warning systems, dynamic risk communication protocols, and the inclusion of island territories in national and European air quality monitoring networks.

In summary, this study contributes new empirical evidence to the limited literature on air pollution in insular regions and underscores the importance of developing tailored, predictive air quality management strategies that reflect the specific vulnerabilities of Atlantic Island environments.

Author Contributions: Conceptualization, M.G.M. and H.C.V.; methodology, M.G.M.; software, M.G.M.; validation, H.C.V.; formal analysis, H.C.V.; investigation, M.G.M.; data curation, M.G.M.; writing—original draft preparation, M.G.M.; writing—review and editing, H.C.V. All authors have read and agreed to the published version of the manuscript.

Funding: This research received no external funding.

Data Availability Statement: No new data were created or analyzed in this study.

Conflicts of Interest: The authors declare no conflicts of interest.

References

1. Kumar, R.P.; Singh, R.; Kumar, P.; Kumar, R.; Nahid, S.; Singh, S.K.; Nijjar, C.S. Aerosol-$PM_{2.5}$ Dynamics: In-situ and satellite observations under the influence of regional crop residue burning in post-monsoon over Delhi-NCR, India. *Environ. Res.* **2024**, *255*, 119141. [CrossRef] [PubMed]
2. Henning, R.J. Particulate Matter Air Pollution is a Significant Risk Factor for Cardiovascular Disease. *Curr. Probl. Cardiol.* **2024**, *49*, 102094. [CrossRef]
3. Nguyen, T.T.N.; Vu, T.D.; Vuong, N.L.; Pham, T.V.L.; Le, T.H.; Tran, M.D.; Künzli, N.; Morgan, G. Effect of ambient air pollution on hospital admission for respiratory diseases in Hanoi children during 2007–2019. *Environ. Res.* **2024**, *241*, 117633. [CrossRef]
4. Vallero, D. Respiratory Effects of Air Pollutants. In *Fundamentals of Air Pollution*, 5th ed.; Academic Press: Cambridge, MA, USA, 2014; pp. 247–256. [CrossRef]
5. Wei, Q.; Chen, Y.; Zhang, H.; Jia, Z.; Yang, J.; Niu, B. Simulation and prediction of PM2.5 concentrations and analysis of driving factors using interpretable tree-based models in Shanghai, China. *Environ. Res.* **2025**, *270*, 121003. [CrossRef]
6. Son, R.; Stratoulias, D.; Kim, H.C.; Yoon, J.-H. Estimation of surface PM2.5 concentrations from atmospheric gas species retrieved from TROPOMI using deep learning: Impacts of fire on air pollution over Thailand. *Atmos. Pollut. Res.* **2023**, *14*, 101875. [CrossRef]
7. Alves, C.; Evtyugina, M.; Vicente, E.; Vicente, A.; Rienda, I.C.; de la Campa, A.S.; Tomé, M.; Duarte, I. $PM_{2.5}$ chemical composition and health risks by inhalation near a chemical complex. *J. Environ. Sci.* **2023**, *124*, 860–874. [CrossRef]
8. Dawidowski, L.; Constantin, J.G.; Murillo, J.H.; Gómez-Marín, M.; Nogueira, T.; Jiménez, S.B.; Díaz-Suárez, V.; Victorica, F.B.; Lichtig, P.; Resquin, M.D.; et al. Carbonaceous fraction in PM2.5 of six Latin American cities: Seasonal variations, sources and secondary organic carbon contribution. *Sci. Total. Environ.* **2024**, *948*, 174630. [CrossRef] [PubMed]
9. Wei, Q.; Zhang, H.; Yang, J.; Niu, B.; Xu, Z. $PM_{2.5}$ concentration prediction using a whale optimization algorithm based hybrid deep learning model in Beijing, China. *Environ. Pollut.* **2025**, *371*, 125953. [CrossRef] [PubMed]
10. Chen, S.; Liu, D.; Huang, L.; Guo, C.; Gao, X.; Xu, Z.; Yang, Z.; Chen, Y.; Li, M.; Yang, J. Global associations between long-term exposure to PM2.5 constituents and health: A systematic review and meta-analysis of cohort studies. *J. Hazard. Mater.* **2024**, *474*, 134715. [CrossRef]
11. Li, H.; Zhang, T.; Su, H.; Liu, S.X.; Shi, Y.Q.; Wang, L.Y.; Xu, D.D.; Zhou, J.M.; Zhao, Z.Z.; Wang, Q.Y.; et al. Factors affecting the different growth rates of $PM_{2.5}$: Evidence from composition variation, formation mechanisms, and importance analysis of water-soluble inorganic ions with case study in northern China. *Atmos. Environ.* **2025**, *340*, 120913. [CrossRef]
12. Zhen, S.; Luo, M.; Xin, F.; Ma, L.; Xu, D.; Cheng, X.; Shao, Y. Chemical composition, source distribution and health risk assessment of $PM_{2.5}$ and PM_{10} in Beijing. *Atmos. Pollut. Res.* **2025**, *16*, 102448. [CrossRef]
13. Canu, I.G.; Wild, P.; Charreau, T.; Freund, R.; Toto, A.; Pralong, J.; Sakthithasan, K.; Jouannique, V.; Debatisse, A.; Suarez, G. Long-term exposure to PM_{10} and respiratory health among Parisian subway workers. *Int. J. Hyg. Environ. Health* **2024**, *256*, 114316. [CrossRef] [PubMed]
14. Kalantary, S.; Jahani, A.; Shams, S.M.P.; Kalantari, B.; Singh, D.; Moeinnadini, M.; Choi, Y. Assessing the effectiveness of artificial neural networks (ANN) and multiple linear regressions (MLR) in forcasting AQI and PM10 and evaluating health impacts through AirQ+ (case study: Tehran). *Environ. Pollut.* **2023**, *338*, 122623. [CrossRef]
15. Alves, C.A.; de la Campa, A.S.; Cipoli, Y.; Furst, L.; Higawa, G.; Leitão, A.; da Silva, A.V.; Feliciano, M.S. PM_{10}-bound elements in Luanda's urban atmosphere: Concentrations, sources, and their environmental and health impacts. *Environ. Pollut.* **2025**, *372*, 125995. [CrossRef]
16. Núñez, A.; Moreno, D.A.; García, A.M. Saharan dust storms affecting the center of the Iberian Peninsula: Effect on the urban aerobiome. *Atmos. Environ.* **2024**, *328*, 120522. [CrossRef]
17. Neff, J.C.; Reynolds, R.L.; Munson, S.M.; Fernandez, D.; Belnap, J. The role of dust storms in total atmospheric particle concentrations at two sites in the western U.S. *J. Geophys. Res. Atmos.* **2013**, *118*, 11201–11212. [CrossRef]
18. Xi, W.; Jie, C.R.; Heng, C.B.; Dong, K.H. Application of Statistical Distribution of PM_{10} Concentration in Air Quality Management in 5 Representative Cities of China. *Biomed. Environ. Sci.* **2013**, *26*, 638–646. [CrossRef]
19. Lu, H.-C. The statistical characters of PM_{10} concentration in Taiwan area. *Atmos. Environ.* **2002**, *36*, 491–502. [CrossRef]
20. Mijić, Z.; Tasić, M.; Rajšić, S.; Novaković, V. The statistical characters of PM_{10} in Belgrade area. *Atmos. Res.* **2009**, *92*, 420–426. [CrossRef]
21. Sánchez, E. Q-Weibull distribution to explain the $PM_{2.5}$ air pollution concentration in Santiago de Chile. *Eur. Phys. J. B* **2023**, *96*, 108. [CrossRef]

22. Kunecki, P.; Franus, W.; Wdowin, M. Statistical study and physicochemical characterization of particulate matter in the context of Kraków, Poland. *Atmos. Pollut. Res.* **2020**, *11*, 520–530. [CrossRef]
23. Yang, Q.; Yuan, Q.; Li, T.; Shen, H.; Zhang, L. The Relationships between $PM_{2.5}$ and Meteorological Factors in China: Seasonal and Regional Variations. *Int. J. Environ. Res. Public Health* **2017**, *14*, 1510. [CrossRef]
24. Pateraki, S.; Asimakopoulos, D.N.; Flocas, H.A.; Maggos, T.; Vasilakos, C. The role of meteorology on different sized aerosol fractions (PM_{10}, $PM_{2.5}$, $PM_{2.5–10}$). *Sci. Total Environ.* **2012**, *419*, 124–135. [CrossRef] [PubMed]
25. Li, X.; Chen, X.; Yuan, X.; Zeng, G.; León, T.; Liang, J.; Chen, G.; Yuan, X. Characteristics of Particulate Pollution ($PM_{2.5}$ and PM_{10}) and Their Spacescale-Dependent Relationships with Meteorological Elements in China. *Sustainability* **2017**, *9*, 2330. [CrossRef]
26. Chen, T.Y.; Chen, S.C.; Wang, C.W.; Tu, H.P.; Chen, P.S.; Hu, S.C.; Li, C.H.; Wu, D.W.; Hung, C.H.; Kuo, C.H. The impact of the synergistic effect of SO_2 and $PM_{2.5}/PM_{10}$ on obstructive lung disease in subtropical Taiwan. *Front. Public Health* **2023**, *22*, 1229820. [CrossRef] [PubMed] [PubMed Central]
27. Wang, L.; Zhao, B.; Zhang, Y.; Hu, H. Correlation between surface PM2.5 and O3 in eastern China during 2015–2019: Spatiotemporal variations and meteorological impacts. *Atmos. Environ.* **2023**, *294*, 119520. [CrossRef]
28. Carvalho, F.; Martins, D.; Meirelles, M.; Vasconcelos, H. Weather and Air Quality Factors Contribution to the Hospital Admissions of Patients with Respiratory Diseases: Case Study of Faial Island (Azores). *Int. J. Environ. Sci. Nat. Resour.* **2022**, *31*, 556305. [CrossRef]
29. Meirelles, M.; Carvalho, F.; Ferreira, A.; Vasconcelos, H.C. Meteorological and Environmental Drivers of Cardiovascular Health Risk in an Insular Region (Azores). *Cardiol. Cardiovasc. Res.* **2025**, *9*, 1–24. [CrossRef]
30. Carvalho, F.; Meirelles, M.; Martins, D.; Vasconcelos, H.C. Yearly Assessment of Weather and Air Quality Impact on Respiratory Disease Hospitalizations: Faial Island (Azores) Study. *Am. J. Health Res.* **2024**, *12*, 165–178. [CrossRef]
31. Meirelles, M.; Carvalho, F.; Porteiro, J.; Henriques, D.; Navarro, P.; Vasconcelos, H. Climate Change and Impact on Renewable Energies in the Azores Strategic Visions for Sustainability. *Sustainability* **2022**, *14*, 15174. [CrossRef]
32. Carvalho, F.S.; Meirelles, M.G.; Henriques, D.; Porteiro, J.; Navarro, P.; Vasconcelos, H.C. Climate Change and Extreme Events in Northeast Atlantic and Azores Islands Region. *Climate* **2023**, *11*, 238. [CrossRef]
33. Available online: https://qualar.apambiente.pt (accessed on 2 March 2025).
34. Abdullah, M.M.; Tan, C.Y.; Ramli, N.A.; Yahaya, A.S.; Fitri, N.F. Modelling of PM10 concentration for industrialized area in Malaysia: A case study in Shah Alam. *Phys. Procedia* **2011**, *22*, 318–324. [CrossRef]
35. Zhang, X.; Liang, H.; Zhong, F.; Liu, Y.; Wang, G. Concentration distribution and cluster analysis of $PM_{2.5}$ based on lognormal cloud model. In Proceedings of the 2022 IEEE 8th International Conference on Cloud Computing and Intelligent Systems (CCIS), Chengdu, China, 26–28 November 2022; pp. 676–683. [CrossRef]
36. Noor, N.M.; Tan, C.Y.; Ramli, N.A.; Yahaya, A.S.; Yusof, N.F. Assessment of Various Probability Distributions to Model Pm10 Concentration for Industrialized Area in Peninsula Malaysia: A Case Study in Shah Alam and Nilai. *Aust. J. Basic Appl. Sci.* **2011**, *5*, 2796–2811.
37. Available online: https://ambiente.azores.gov.pt/qualidadedoar/Default.aspx (accessed on 24 March 2025).
38. Lu, H.-C.; Fang, G.-C. Predicting the exceedances of a critical PM10 concentration—A case study in Taiwan. *Atmos. Environ.* **2003**, *37*, 3491–3499. [CrossRef]
39. Decreto Legislativo Regional nº 32/2012/A, Diário da República 1ª Série, 135, 3706. Available online: https://files.diariodarepublica.pt/gratuitos/1s/2012/07/13500.pdf (accessed on 25 March 2025).
40. Portuguese Environment Agency (APA). Available online: https://ambiente.azores.gov.pt/qualidadedoar/store/Uploads/AlertasNotas/previsao_en_2024_01_26_acores.pdf (accessed on 30 March 2025).
41. Portuguese Environment Agency (APA). Available online: https://ambiente.azores.gov.pt/qualidadedoar/store/Uploads/AlertasNotas/previsao_en_2024_01_27_acores.pdf (accessed on 30 March 2025).
42. Portuguese Environment Agency (APA). Available online: https://ambiente.azores.gov.pt/qualidadedoar/store/Uploads/AlertasNotas/previsao_en_2024_02_02.pdf (accessed on 30 March 2025).
43. Portuguese Environment Agency (APA). Available online: https://ambiente.azores.gov.pt/qualidadedoar/store/Uploads/AlertasNotas/previsao_en_2024_02_04.pdf (accessed on 30 March 2025).
44. Portuguese Environment Agency (APA). Available online: https://ambiente.azores.gov.pt/qualidadedoar/store/Uploads/AlertasNotas/previsao_en_2024_02_05.pdf (accessed on 30 March 2025).
45. Portuguese Environment Agency (APA). Available online: https://ambiente.azores.gov.pt/qualidadedoar/store/Uploads/AlertasNotas/previsao_en_2024_02_06.pdf (accessed on 30 March 2025).
46. Portuguese Environment Agency (APA). Available online: https://ambiente.azores.gov.pt/qualidadedoar/store/Uploads/AlertasNotas/previsao_en_2024_04_14.pdf (accessed on 25 April 2025).
47. Portuguese Environment Agency (APA). Available online: https://ambiente.azores.gov.pt/qualidadedoar/store/Uploads/AlertasNotas/previsao_en_2024_04_15.pdf (accessed on 25 April 2025).

48. Portuguese Environment Agency (APA). Available online: https://ambiente.azores.gov.pt/qualidadedoar/store/Uploads/AlertasNotas/previsao_en_2024_04_16.pdf (accessed on 25 April 2025).
49. Portuguese Environment Agency (APA). Available online: https://ambiente.azores.gov.pt/qualidadedoar/store/Uploads/AlertasNotas/previsao_en_2024_11_11.pdf (accessed on 25 April 2025).
50. Portuguese Environment Agency (APA). Available online: https://ambiente.azores.gov.pt/qualidadedoar/store/Uploads/AlertasNotas/previsao_en_2024_12_27.pdf (accessed on 25 April 2025).
51. Portuguese Environment Agency (APA). Available online: https://ambiente.azores.gov.pt/qualidadedoar/store/Uploads/AlertasNotas/previsao_en_2024_12_28.pdf (accessed on 25 April 2025).
52. Portuguese Environment Agency (APA). Available online: https://ambiente.azores.gov.pt/qualidadedoar/store/Uploads/AlertasNotas/previsao_en_2024_12_29.pdf (accessed on 25 April 2025).

Disclaimer/Publisher's Note: The statements, opinions and data contained in all publications are solely those of the individual author(s) and contributor(s) and not of MDPI and/or the editor(s). MDPI and/or the editor(s) disclaim responsibility for any injury to people or property resulting from any ideas, methods, instructions or products referred to in the content.